MICROSTRUCTURAL AND MECHANICAL CHARACTERIZATION OF METAL ACTIVE GAS WELDED JOINT BETWEEN CAST IRON AND LOW CARBON STEEL

A THESIS SUBMITTED TO
THE GRADUATE SCHOOL OF NATURAL AND APPLIED SCIENCES
OF
MIDDLE EAST TECHNICAL UNIVERSITY

BY

MURAT TOLGA ERTÜRK

IN PARTIAL FULFILLMENT OF THE REQUIREMENTS
FOR
THE DEGREE OF MASTER OF SCIENCE
IN
METALLURGICAL AND MATERIALS ENGINEERING

FEBRUARY 2011

Approval of the thesis

MICROSTRUCTURAL AND MECHANICAL CHARACTERIZATION OF METAL ACTIVE GAS WELDED JOINT BETWEEN CAST IRON AND LOW CARBON STEEL

Submitted by **MURAT TOLGA ERTÜRK** in partial fulfillment of the requirements for the degree of **Master of Science in Metallurgical and Materials Engineering Department, Middle East Technical University** by

Prof. Dr. Canan Özgen
Dean, Graduate School of **Natural and Applied Sciences** _____

Prof. Dr. Tayfur Öztürk
Head of Department, **Metallurgical and Materials Eng.** _____

Prof. Dr. Rıza Gürbüz
Supervisor, **Metallurgical and Materials Eng. Dept., METU** _____

Dr. Caner Batıgün
Co-Supervisor, **Weld. Tech. and NDT Res./App. C., METU** _____

Examining Committee Members

Prof. Dr. Bilgehan Ögel
Metallurgical and Materials Eng. Dept., METU _____

Prof. Dr. Rıza Gürbüz
Metallurgical and Materials Eng. Dept., METU _____

Prof. Dr. C. Ali Kalkanlı
Metallurgical and Materials Eng. Dept., METU _____

Assist. Prof. Dr. Kazım Tur
Materials Engineering Department, Atılım University _____

Dr. Caner Batıgün
Welding Tech. and NDT Res./App. C., METU _____

Date: 08/02/2011

I hereby declare that all information in this document has been obtained and presented in accordance with academic rules and ethical conduct. I also declare that, as required by these rules and conduct, I have fully cited and referenced all material and results that are not original to this work.

Name, Last name: Murat Tolga ERTÜRK

Signature:

ABSTRACT

MICROSTRUCTURAL AND MECHANICAL CHARACTERIZATION OF METAL ACTIVE GAS WELDED JOINT BETWEEN CAST IRON AND LOW CARBON STEEL

Ertürk, Murat Tolga

M. Sc., Department of Metallurgical
Supervisor : Prof. Dr. Rıza Gürbüz
Co-supervisor : Dr. Caner Batıgün

February 2011, 82 Pages

This study focuses on joining pearlitic ductile cast iron with low carbon steel by welding and investigation of this joint in microstructural and mechanical viewpoints. For this purpose E355 steel and GJS600-3 cast iron were joined using metal active gas (MAG) welding process by G3Si1 filler wire. The joining process is shaped mainly by the problems related to the low weldability of cast. Preheating was applied to prevent formation of cooling cracks and effects of post weld heat treatments (PWHT) were surveyed. Micro examination and micro hardness tests were applied to characterize the general microstructure. Grain size measurements were done for E355. Hardness profiles, tension and impact toughness properties were designated via mechanical tests. Fatigue behavior was surveyed and general fracture

characteristics were determined via scanning electron microscopy (SEM) examinations.

According to study it was concluded that successful weld joint could be formed between the materials by suitable preheating. Formation of ledeburitic white cast iron and martensite in heat affected zone of cast piece was witnessed. It was possible to lower high hardness values of these phases gradually by increasing post weld heat treatment temperatures. The weld joint behaved superior to the base metals under tension and fatigue tests. In tension tests failure occurred at E355 base metal whereas fatigue loading resulted failure at GJS600-3. A great impact toughness variation was determined between two pieces. It is seen that heat treatments had minor effect on mechanical test results except hardness. The study was concluded that a useful fusion weld joint between these materials can be built.

Keywords: MAG welding, nodular cast iron, E355, microstructure, fatigue

ÖZ

DÖKME DEMİR VE DÜŞÜK KARBONLU ÇELİK ARASINDAKİ METAL AKTİF GAZ KAYNAĞI BİRLEŞTİRMESİNİN İÇYAPISAL VE MEKANİK KARAKTERİZASYONU

Ertürk, Murat Tolga

Yüksek Lisans, Metalürji ve Malzeme Mühendisliği Bölümü
Tez Yöneticisi : Prof. Dr. Rıza Gürbüz
Ortak Tez Yöneticisi : Dr. Caner Batıgün

Şubat 2011, 82 Sayfa

Bu çalışma perlitik küresel dökme demirin düşük karbonlu çelik ile kaynak yolu ile birleştirilmesine ve bu birleşmenin mikroyapı ve mekanik özelliklerinin incelenmesine odaklanmıştır. Bu amaç için, metal E355 çeliği ve GJS600-3 dökme demir G3Si1 dolgu malzemesi ile metal aktif gaz (MAG) kaynağı kullanılarak birleştirilmiştir. Birleştirme işlemi genel olarak dökme demirin düşük kaynaklanabilirliğinden kaynaklanan sorunlara göre şekillendirilmiştir. Soğuma çatlamalarının önlenmesi için ön ısıtma uygulanmış, kaynak sonrası ısıl işlemin etkileri incelenmiştir. Mikroyapı incelemeleri ve mikro sertlik testleri uygulanarak kaynağın genel mikroyapısı sınıflandırılmış ve çelik parça için tane boyutu ölçümleri yapılmıştır. Mekanik testler ile kaynağın sertlik profilleri, çekme ve darbe özellikleri belirlenmiştir. Yorulma davranışları belirlenmiş ve tarama elektron mikroskobu kullanılarak kırılma karakterleri belirlenmiştir.

Uygun ön ısıtma uygulanarak iki malzemenin başarı ile birbirine kaynaklanabilmiştir. Dökme demirin ısıdan etkilenmiş bölgesinde ledebüritik beyaz dökme demir ve martensit oluşumuna rastlanmıştır. Bu fazların sebep olduğu yüksek sertlik değerleri kaynak sonrası ısıl işlem sıcaklıkları arttırılarak aşama aşama düşürülebilmiştir. Çekme ve yorulma deneylerinde kaynak birleştirmesi ana malzemelerden daha üstün mekanik davranışlar sergilemiştir. Çekme testlerinde kırılma E355 ana malzemesinde oluşurken yorulma testleri GJS600-3 ana malzemesinde kırılmaya neden olmuştur. İki malzeme arasında ciddi darbe tokluğu farklılığına rastlanmıştır. Isıl işlemlerin sertlik dışındaki mekanik test sonuçlarına etkisi olmadığı görülmüştür. Çalışma, iki malzeme arasında kullanılabilir bir eritme kaynağı birleştirmesinin oluşturulabileceği ile sonuçlandırılmıştır.

Anahtar Kelimeler: MAG kaynağı, küresel dökme demir, E355, mikro yapı, yorulma

Masakatsu Agatsu

AKNOWLEDGEMENTS

I would like to express my deepest graduate to my thesis supervisor Prof. Dr. Rıza Gürbüz for his valuable guidance and supervision.

I would also like to thank to my thesis co-supervisor Dr. Caner Batıgün for leading and supporting me all through the study.

I am grateful to İbrahim Korkmaz and Ozan Alçiçek from TOFAŞ for their inspiration about this study and their support on the work.

I am also grateful to Dr. Önder Orhaner and Utku Uygur from Akdaş Casting Ind. & Trade Co. for providing cast materials required for the study.

My special thanks go to all the members of METU Welding Technology and Non-Destructive Testing Research and Application Center for creating limitless opportunities for my studies and for their priceless efforts.

Guidance and helps of Dr. Süha Tirkeş and Koray Yurtışık are gratefully and respectfully acknowledged.

I also appreciate valuable efforts of Göksu Gürer for his efforts and helps on mechanical tests.

I want to thank Mert Akkuş, Sinan Değer, Murat Ekşi, Cihangir Tezcan, Derya Erdem for their friendship and support and especially their valuable sharing of the good and bad times of the path.

I want to extend my appreciation to Ümit and Nurşen Acar Dedeoğlu, my sensei Bora Açıkalın and my fellow aikidokas, to all my friends and to whomever eased the load on me walking this path.

Finally I would like to thank my parents Tülay and Şükrü Ertürk and my brother Özgür Ertürk for their support and patience.

TABLE OF CONTENTS

LIST OF TABLES

TABLES

LIST OF FIGURES

FIGURES

CHAPTER 1

INTRODUCTION

Nearly all of the productions in today's world, from the simplest to the most complicated, are all composed of the combination of smaller parts or elements together. It is almost all the time neither feasible nor even possible to make productions in a single step. Thus people were and are always in need of successful and efficient joining processes since ancient times. Especially with the improvement of the technology, as the productions get more detailed and more complicated, joining of elements having different types, kinds and structures become necessary.
In order to build the designed structures, a large variety of different joining methods were developed. Among these, especially for joining of metals, welding was found its way through vast areas of today's industry and become the most used joining method.

The definition of welding can be expressed as forming an atomic bonding configuration having a natural electron configuration between to materials by bringing their surfaces together. Thus any process causing materials to join through inter-atomic or inter-molecular forces can be regarded as welding [1]. With this point of view, very different welding methods coming from the historical times to today's modern days can be imagined, understood and the greatness of the coverage areas of welding can be judged.

When glanced through the history, the earliest evidence of welding can be seen in Bronze Age and Iron Age but the first famous construction that is put together by the ancient welding methods is the Iron Pillar in India which is erected at about 310AD [2]. Welding was applied as the heating and forging of the metals through the Middle-Ages and to Renaissance. With the development of technology and the

driving forces of the World Wars fusion welding processes were invented and developed in the 19th and 20th centuries. By the catastrophic failures of bridges, pressure vessels and Liberty ships that took place during 1930s and 1950s importance of welding quality was understood and studies were started to concentrate on the subject. As a result welding was started to be used as the main means of assembly after the 1950s thanks to these studies born from the disasters [3]. All these failures occurred in history are the proof that though a very common and practical process, welding should be applied with the support of very detailed and meticulous studies.

Among the studies related to the welding, this present study focuses on optimizing the weld quality between ductile cast iron and low carbon steel. The idea was introduced by TOFAŞ with the aim of producing certain load bearing elements used in automobiles in an easier and economical method. The technical aim of the project is to build a cast element having complicated geometry in two pieces made of cast iron and low carbon steel, which are joined by a successful welding operation. By such a joint, production of a lighter and more economical structure was aimed.

Additionally, these two material types can be counted as the fundamental building blocks of most of the structures used in today's world. In most of the land and sea vehicles, buildings and especially in the automotive industry both find their uses in the same structure. In such cases a successful welding operation can be thought of a joining method to hold these materials together.

It is possible to have successful welded joints between these materials individually (cast iron to cast iron or steel to steel), but in both of these cases separate paths should be followed to reach success. Especially cast iron requires more detailed and cumbersome processes whereas low carbon steels can be welded with small precautions without problems. This study aims to unite these welding paths in the simplest and more economical way. The main points to be taken into account are creating a weld joint providing the welding requirements of the base metals, having homogeneous material properties along the weld zone and at the same time causing no damage or degradation to the base materials.

The main cause of the problems of welding regarding these two material groups is the large difference of the carbon content. High amount of carbon in the cast iron and high cooling rates of welding operation causes formation of very hard and brittle structures and the material becomes susceptible to cracking upon cooling. In order to achieve a joint without defects and control of the micro-structure and thus hardness and mechanical properties of the weld zone suitable post and preheating operations should be applied.

In this study welding of these materials was studied in three main steps. Initially, materials' reactions to the different welding parameters were determined; secondly weld joints having no discontinuities were produced; finally mechanical properties in accordance with the micro-structure of the work pieces were examined. In order to achieve these steps, bead on plate welding, pre-heating, post weld heat treatment, macro and micro examination, hardness and micro hardness tests, fatigue tests, scanning electron microscopy (SEM) examinations were carried out step by step.

CHAPTER 2

THEORY

2.1 Cast Iron

Cast irons are the ferrous alloys having carbon content generally greater than 2.1 wt% and solidifying with a eutectic structure. By the eutectic solidification characteristics, cast irons can be liquid between 1150-1300°C and shows good fluidity and casting characteristics, making melting and casting a preferable production technique.

According to the composition and the cooling rate during welding cast irons may solidify with respect to the thermodynamically metastable Fe-Fe_3C or stable Fe-Graphite systems. There forms a considerable difference between the stable and the metastable solidification types in mechanical properties. Because of this reason, in production, type of eutectic solidification should tried to be controlled. General cast iron types and their production routes can be seen in Figure 1 and Figure 2.

2.1.1 White Cast Iron

When the cooling is rapid, the carbon cannot form graphite instead remains as metastable iron carbide and large amounts of cementite is formed. Also graphitization may be inhibited by the alloy composition. The structure is very hard and brittle and unmachinable but can be used as a wear resistive material.

2.1.2 Malleable Cast Iron

If suitable heat treatment is applied to the white cast iron, annealing at 800-900°C for prolonged times, the carbon in the cementite precipitates as graphite having irregular

shapes. The structure of matrix is determined by annealing process as ferrite or pearlite. Malleable cast irons yield high strengths and appreciable ductility.

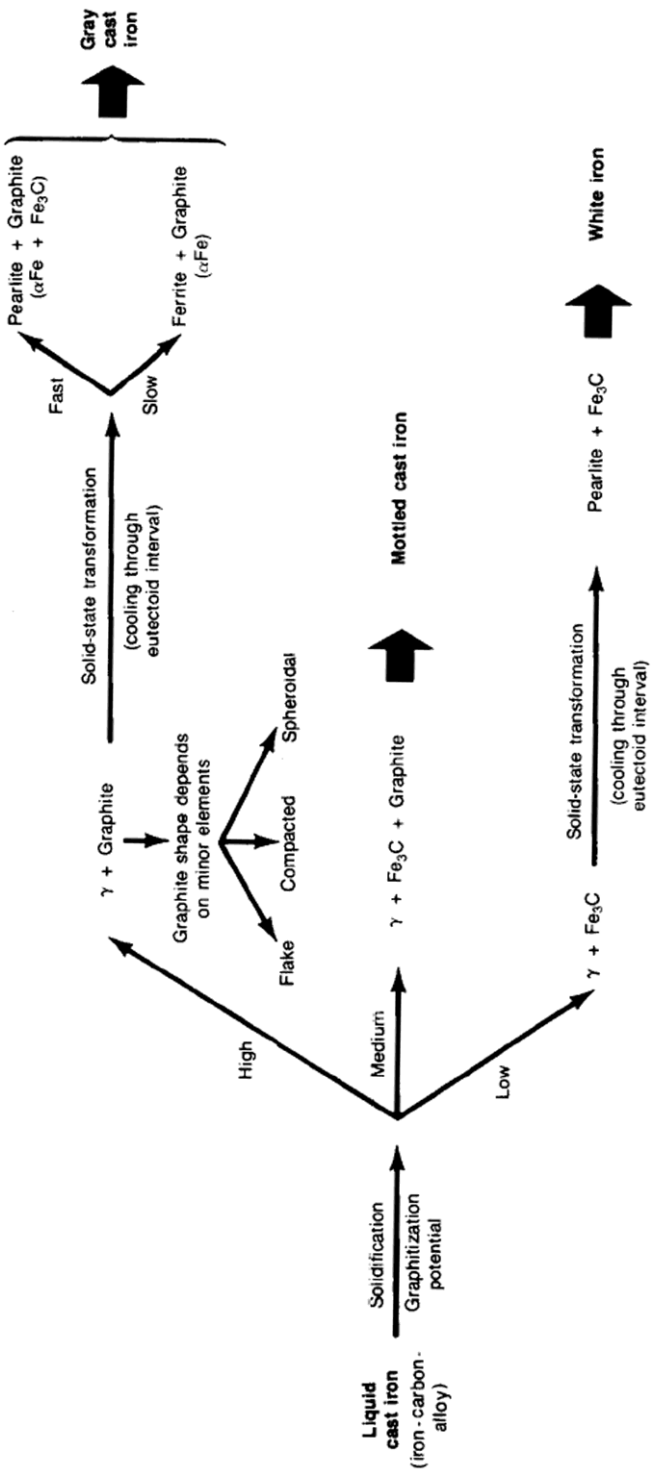

Figure 1 Basic microstructures and processing for obtaining common commercial cast irons (part 1) [4]

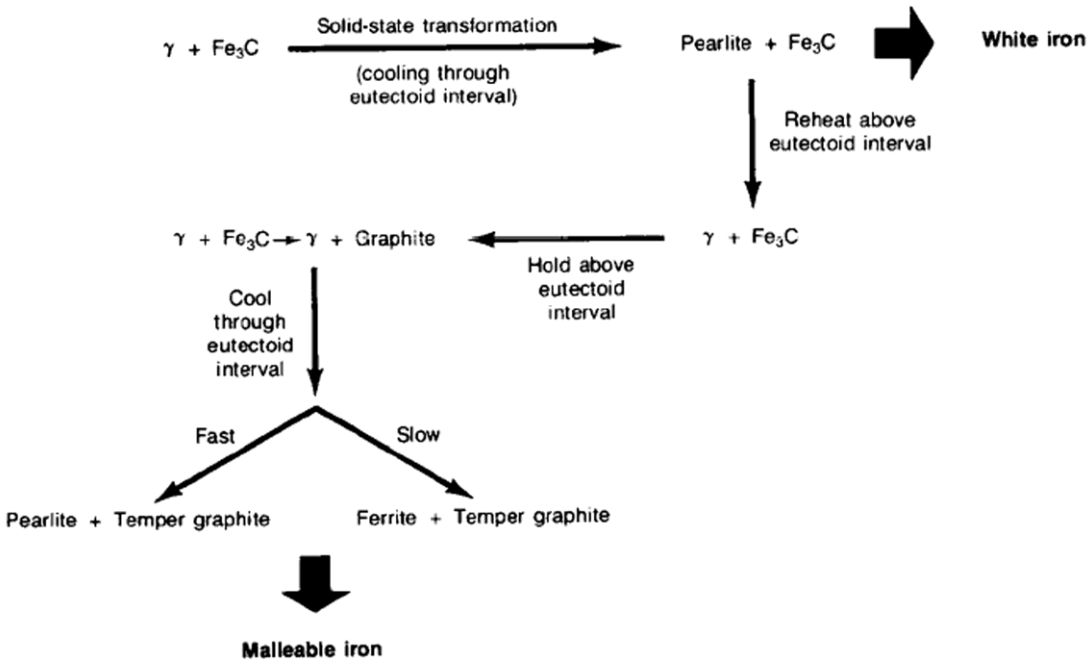

Figure 2 Basic microstructures and processing for obtaining common commercial cast irons (part 2) [4]

2.1.3 Gray Cast Iron

Gray cast iron is the most common type of cast iron. Generally it has about 1 - 3 wt% Si. Presence of silicon in combination with the slow cooling promotes the formation of graphite instead of iron carbide. In this type, graphite is in the form of flakes. Typical flake structure can be seen in Figure 3. General microstructure of gray cast irons consists of flakes distributed in pearlitic matrix but addition of about 15% Ni to the composition may produce austenitic matrix. In fast cooling rates free cementite, and in slow cooling rates free ferrite is produced in the microstructure.

The graphite flakes behave like the cracks in the microstructure therefore gray cast irons show weak mechanical characteristics in tension whereas possess high strength in compression. White cast irons show good damping capacities and wear resistances. Additionally high fluidity at casting temperature promotes casting of complex shapes. Most importantly white cast iron is the cheapest among the metallic materials.

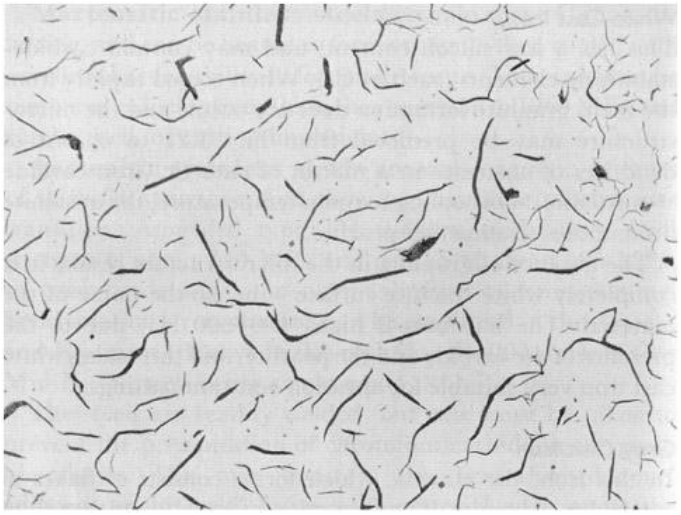

Figure 3 Optical micrograph of grey cast iron, unetched (x500) [5]

2.1.4 Nodular Cast Iron

Nodular cast irons are produced adding magnesium or cerium to the gray iron composition. These elements act as nodulizers and change the flake like morphology of graphite into nodules, which can be seen in Figure 4. Therefore the crack behavior of the graphite gets eliminated and the mechanical properties, especially in tension become improved. Mechanically nodular cast irons may have characteristics similar to steels. Thus, they combine the advantageous properties of steels and cast irons.

Graphite nodules dispersed into pearlitic and/or ferritic matrix constructs the characteristic microstructure of nodular cast irons. Generally the nodules are surrounded by ferrite in the pearlitic matrix, constructing Bull's-eye structure. If the material is annealed, secondary graphite forms surrounding the already present primary graphite nodules and the matrix becomes ferritic. [1,5, 6, 7, 8]

2.2 Welding

Welding is the most used and practical joining method that is used in the industry. In today's world the traces of welding can be seen nearly in all the branches of production. The buildings, bridges, aerospace vehicles, automobiles, elements of defensive industry, street lamps, petroleum pipelines, sewer systems, most of the everyday use items etc. are all held together by various kinds of welding processes. The effect of welding in our daily life cannot in any degree be denied. It can clearly

be judged that from the day the welding processes started to find body in industry, they have made it possible to increase the quality of the life. So in welding point of view, in order to improve the quality of life, quality of weldments should be increased.

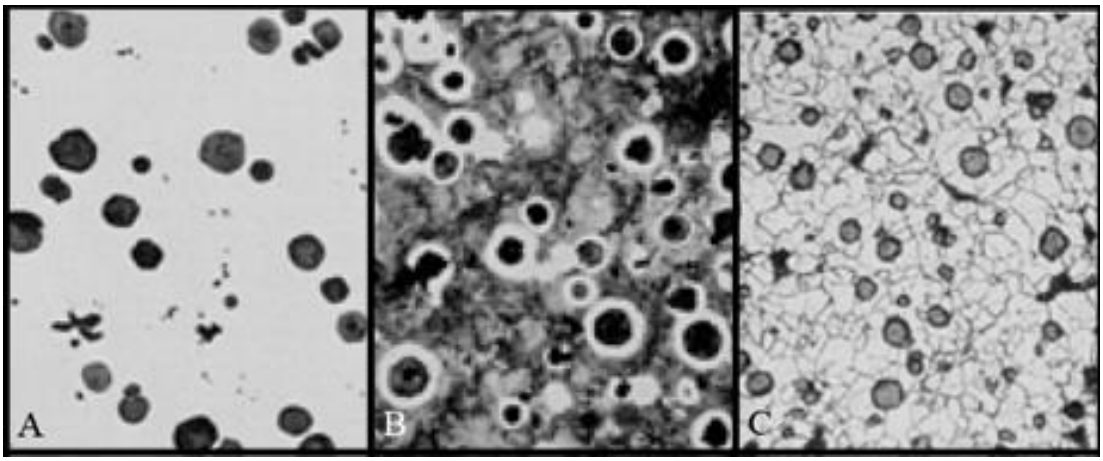

Figure 4 Typical micro-structure of nodular cast iron. A) graphite nodules, unetched, 100x; B) typical bull's-eye structure of graphite nodules surrounded by ferrite in matrix of pearlite; C) annealed and furnace cooled nodular cast iron, most of the original pearlite has decomposed into a matrix of free ferrite (light) and pearlite (black, irregular) [6]

In very basic terms, welding constitutes a continuous solid body from two separate pieces. The main point in welding is to bring the two surfaces of the materials together so close that a new atomic arrangement can be formed between two items. This requires atomic distance between the surfaces and requires very cumbersome surface preparation like polishing and cleaning the surfaces off the possible obstacles that may prohibit joining. Among various methods, to ease the joining surfaces together, people have found fusion to be the most effective one. The materials to be joined are melted and upon solidification of the molten bath in between, the atomic bonds and thus the continuous work piece are formed. And as the nature of the process, this type is named as fusion welding [3].

2.2.1 Arc Welding

In arc welding, an electric arc is created between the work piece and the electrode. The arc produced is used as the heat source for melting of the materials. In arc welding additional mechanical pressure or filler materials may be or may not be used.

In this process the electrode may be consumable or non-consumable. The consumable electrodes can be mechanically fed into the weld pool or it may be in the shape of a rod which manually fed during the welding. Hence, the consumable electrodes also work as filler materials. In the case of non-consumable electrodes, carbon or tungsten may be used. In this type, if required, filler materials may be supplied to the welding as wires or rods electrode is used just for starting the arc [9].

In arc welding the weld bath can be protected from the atmosphere by the protective gases, fluxes or slag producing covers of the electrodes. These protective elements both prevent corrosion and improve the weld quality.

2.2.1.1 Metal Active Gas (MAG) Welding

In MAG welding process the arc is created between the continuously fed filler wire and the metals to be welded. With the heat of the arc the filler wire is melted and deposited on the weld bath. The shielding gases which, as mentioned above, both protect the weld pool from the atmosphere and modify the arc characteristics are supplied to the system externally by the welding torch. Typical structure of MAG torch can be seen in Figure 5.

According to the type of the gas used in the process the characteristics of the weld changes. When inert gases like argon or helium or mixture of both are used the process is called Metal Inert Gas (MIG) welding. Argon here stabilizes the arc and gives a focused penetration depth. With the increase of Ar content in the protective gas mixture the penetration of the weld becomes more like a papillary type however; He gives a parabolic type penetration (Figure 6). MIG welding is most commonly used for welding aluminum and its alloys [11,3].

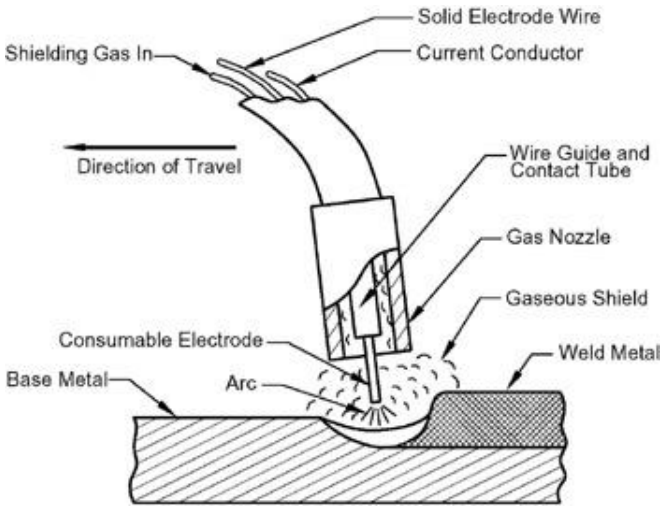

Figure 5. MIG/MAG Torch [10]

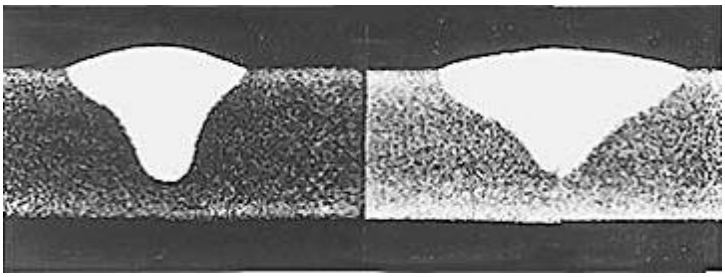

Figure 6. MAG welds in 6.4 mm thick 5083 Al made with Ar (left) and 75% He-25% Ar (right) [11]

In addition to inert gases, the mixture of active gases, like O_2 and CO_2, to Ar changes the process to Metal Active Gas (MAG) welding. Addition of these gases enables stabilization of the arc for broader range of weld power parameters, provides more fluid weld baths, decreases void formation, increases the penetration and also reduces the cost of the protective gas. In addition to these advantages when working with ferrous materials formation of spatters and undercuts due to the He and Ar content makes MAG the usual choice [11,3].

According to the welding parameters, used electrodes and shielding gases the metal transfer can be various between three types as spray, globular, short circuiting transfer.

Spray Transfer can be achieved when using argon rich shielding gas, direct current electrode positive power, and a current level above a critical value which is called as transition current which is dependent upon the material to be welded, electrode diameter and protective gas composition. Below this current level the transfer mode becomes globular. With this method creation of small droplets reaching rates of more than several hundred per second is possible. In this mode the transfer is stable and spatter formation is reduced very effectively [11,9,10].

In *globular transfer* the filler material melts and forms drops at about the size of the diameter of the filler wire. When CO_2 and He is used as the shielding gas these form of transfer can be obtained in all usable welding currents. This mode causes considerable amount of spatter [11]. Even burying the arc below the surface cannot prevent formation of spatters [9].

Short Circuiting Transfer, as the name indicates, occurs when the electrode tip touches to the weld pool and a short circuit is created. In this method very low current values are used and this method causes low heat inputs and creates small weld pools and low penetration. These properties of short circuiting transfer enable this method to be used welding thin sections [11,9,10].

2.3 Welding of Cast Iron

The problematic welding characteristics of the cast iron originate majorly from the high carbon content of the material. Upon welding and cooling, the carbon makes formation of various undesired microstructures possible, reducing the weldability a great deal in all regions related to welding.

There are two possible routes for welding cast irons which are named as cold and hot welding. These two methods are primarily separated from each other according to the preheating temperatures ranges. In cold welding preheating values lower than 300°C are applied while hot welding required preheating higher than 300°C, commonly at the range of 500°C.

In cold welding, the lower preheating temperatures are not sufficient for lowering the cooling rate to the desired values and hence formation of brittle phases as martensite and carbides are encountered. For these cases generally Ni based electrodes are used.

Ni based fillers are weaker than steel alloys and yields higher ductility. Increased ductility suspends crack formation especially in case of martensitic transformation and additionally Nickel bonds with Carbon preventing formation of iron carbide. Despite these superior properties, Ni electrodes provide relatively lower mechanical properties with respect to steel.

When cast iron weldments are required to be operated at higher stress values, filler materials with similar properties to base metal are chosen. In order to prevent the formation of possible brittle phases with such fillers, the preheating temperatures get increased and these processes are named as hot welding.

As in any welding operation the temperature gradient over the material causes formation of characteristic regions of weldments as weld metal, and HAZ. But for cast irons, HAZ can be divided into unmixed zone (UMZ), partially melted zone (PMZ) and true HAZ (Figure 7).

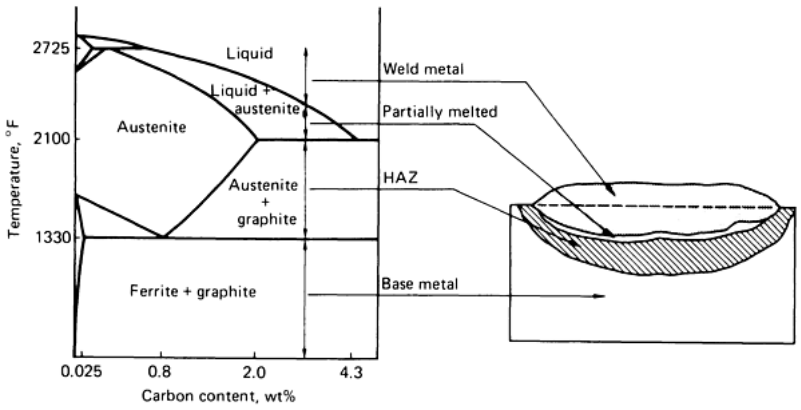

Figure 7. Schematic representation of the temperature zones in a typical cast iron welding [8]

In fusion zone, the molten metal cools very rapidly due to the nature of welding, and in this short time the carbon becomes trapped and cannot form graphite, instead iron carbide or martensite formation is possible. These phases make weld metal

susceptible to cracking. Formation of these structures is directly related to filler material composition and the alloying ratios.

In unmixed zone the base material melts but mixture with weld pool cannot be achieved. Because of lack of mixing no alloying can be achieved. The solidified structure is only characterized by cooling rates. Again in this zone white cast iron and martensite formation occurs. Formation of this region cannot be prevented; only by increasing convection the amount can be reduced.

Neighboring unmixed zone, partially melted zone can be determined, in which the base metal is only partially melted. This region reaches to the temperatures in between the liquidus and solidus lines of the related composition as shown in Figure 7. Due to high cooling rates white cast iron formation can be observed in PMZ. Also very complex and problematic structures can be formed in this region. Holding the peak temperatures during welding as low as possible is the best option to reduce cracking problems of this region which may be helped by preheating and filler metal types.

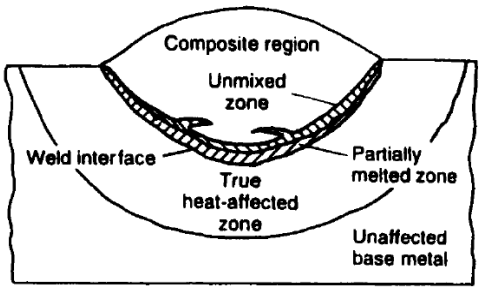

Figure 8. Schematic showing the different discrete regions present in a single-pass fusion weld, including the unmixed zone [8]

As a summary the rapid solidification of the cast iron almost always causes undesired structures for welding. This formation can be modified by alloying elements in the melt region but it is always more problematic to control the interior melted regions. Hence in cast iron weldments both filler materials and control of cooling rates play very important roles.

Getting further away from the weld seam, the temperatures become insufficient for melting but sufficient for phase changes. This region can be called as true HAZ. The main problem here is the martensitic transformation. Cooling rates again become the most important factor here [12,8,13].

The schematic representation of all these zones is shown in Figure 8.

2.4 Weldability of Cast Iron

Weldability of the cast iron is commonly characterized by calculation of the carbon equivalent (CE). By CE no-crack temperature for the cast iron is determined. No-crack temperature is the preheating temperature, above which the cooling rates will be lowered enough that the material will not cause formation of any cracks due to welding. CE is calculated using the weight percents of the elements in the chemical composition according to Equation 1 [8] below:

$$CE = C + 0.31Si + 0.33P + 0.45S - 0.028Mn + Mo + Cr - 0.02Ni - 0.01Cu \quad (1).$$

The no-crack temperature is correlated with the CE by Figure 9. The lower the no-crack temperature is the more weldable the cast iron is. Here the preheating is determined by CE and main structure of the cast iron to be welded.

Additionally, the thickness of the material will be another factor determining the cooling rate after welding. Increased thickness causes an increase in cooling rates thus weldability of the thicker pieces will be lower requiring increased preheating temperatures.

2.5 Dissimilar Metal Fusion Welding

Dissimilar metal welding is joining two metals or alloys with different chemical compositions by welding. Welding of Al to Cu or welding of different alloys of same metal can be considered as dissimilar welding. In such cases because of the natures of the materials to be welded, certain risks can be encountered during joining. These risks can arise from melting point, thermal expansion coefficient and thermal conductivity variations and general alloying and precipitation problems of the metals.

In dissimilar metal welding, the chemical composition may show regional diversities because of the **alloying problems**. Especially when multi-pass welding is carried out it is expected to come across such differences in the composition at the base metal boundary regions. Also because of insufficient mixing, macro segregation can be come across. Such composition diversities in the material may result different cooling characteristics and can be responsible for cracks upon solidification. In addition to the base materials another solubility problem can be introduced from the filler materials. A filler composition capable of alloying both base materials tried to be chosen in order to reduce the risks mentioned however; the filler should also satisfy strength at least higher than the weaker of the materials to be welded.

Another source for dissimilar welding problems is the **dissimilar melting temperatures** of the metals to be joined. Because of the difference in melting temperatures, during melting or cooling, one of the materials may be in solid state while the other is solid. In such case, during solidification, the shrinkage of the already solid metal may induce stresses on the still solidifying low melting constituent. These stresses may result tearing of the metal with the low melting point. This problem may be overcome with application of buttering which is deposition of the metal surface by another metal having intermediate melting temperature. By this solution, the melting temperature variation between the two metals is lowered and stress affecting on the solidifying metal is lowered.

Thermal expansion coefficient differences between the metals also acts like the melting temperature variations. Even if the materials have very similar melting temperatures, a large difference in thermal expansion coefficients may cause tearing of one of the metals during solidifying. That is because of the effect of tensile and compressive forces aroused of expansion. The material under effect of tension is under the risk of tearing.

For the case of **thermal conductivity differences**, the better conductor material will absorb a greater proportion heat and the heat distribution during the welding will be non-homogeneous even with the materials having identical geometries. This problem may cause lack of fusion. In this case, heat balance should be well configured by suitable heat treatments. [5]

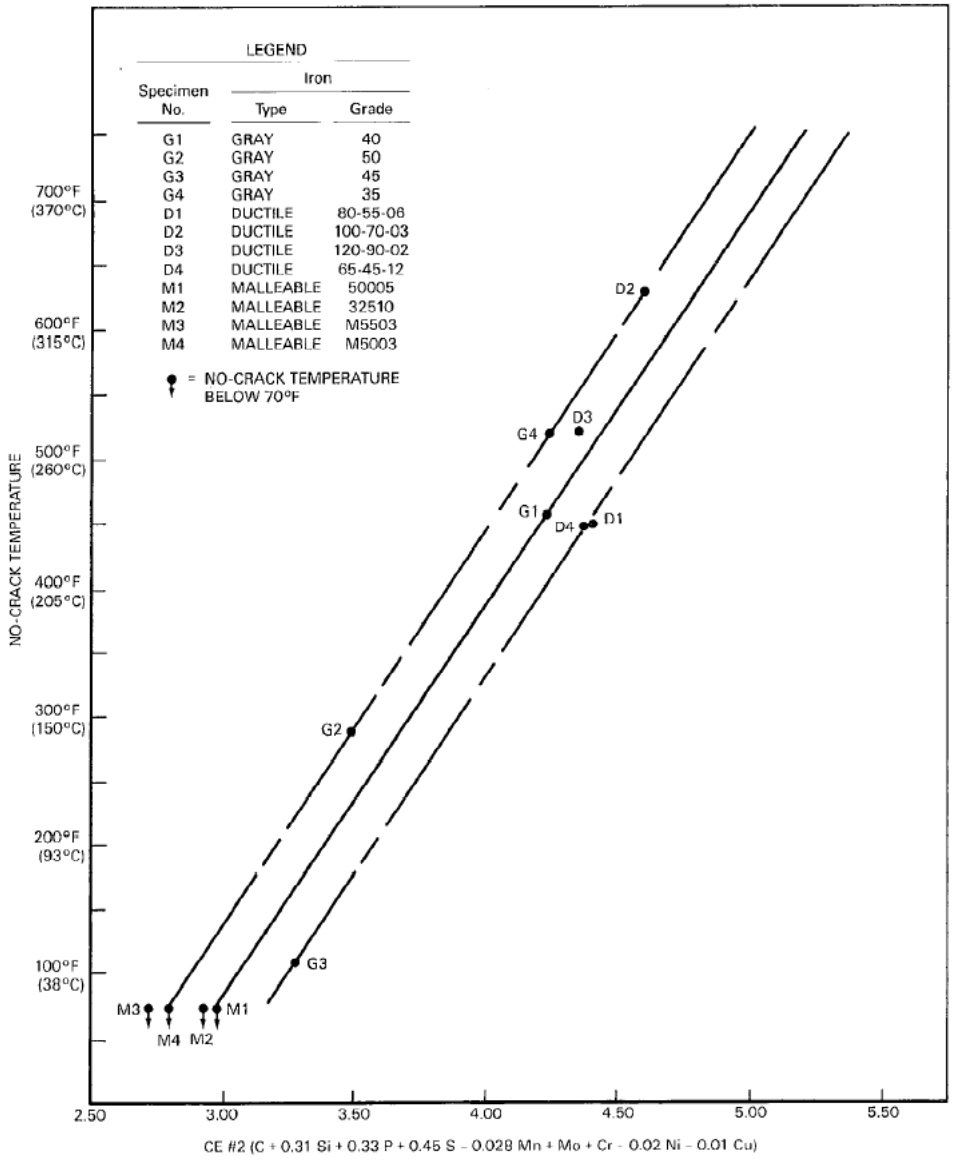

Figure 9. Effect of CE on no-crack temperature for selected grades of iron castings [12]

2.6 Fatigue Behavior of the Welded Joints

The certain factors affecting the fatigue behavior of any material are also valid for the welded joints. These factors related to the fatigue life can be summarized as characteristics of the material, geometry of the material, residual stresses, production and surface quality and environmental service conditions. When a weld is introduced the geometry and surface quality degrade, characteristics change and appreciable

residual stress is added to the material. These factors can be summarized using Figure 10 and Figure 11.

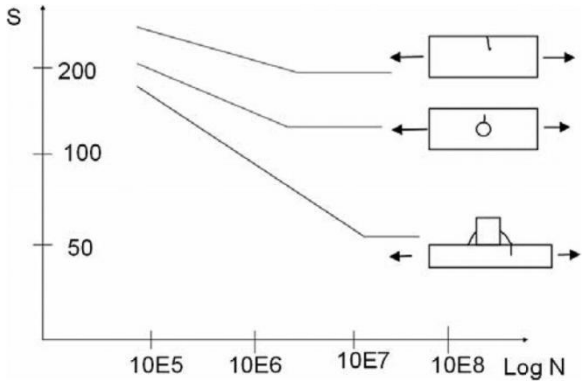

Figure 10 Fatigue life curves for various details [14]

Figure 10 shows typical S-N curves of smooth plate, a plate with a hole introduced in middle and a fillet welded joint with the crack initiation locations. In this loading condition the fillet weld is referred as non-load carrying because the load acts straight through the base plate. Although in non-load carrying condition the welded joint has even shorter fatigue life than the plate with the bore hole which has a stress concentration factor close to 3 as represented in Figure 11.

In this case the weld geometry creates a notch effect which is directly related to the flank angle shown as θ in Figure 11 and the perpendicular welded plate also increases the stress concentration the weld metal geometrical factor being the most important one. This geometry can be softened by increasing the toe radius, ρ and decreasing the angle α. But these two values will vary along the weld and hence will not be controllable.

Even if the notch effect is decreased to comparable values to the bore hole, there are still residual stresses and possible micro flaws introduced to the surface by welding to be considered. Combination of these factors at same point causes serious decrease in the fatigue life of the material and this point becomes the location of failure.

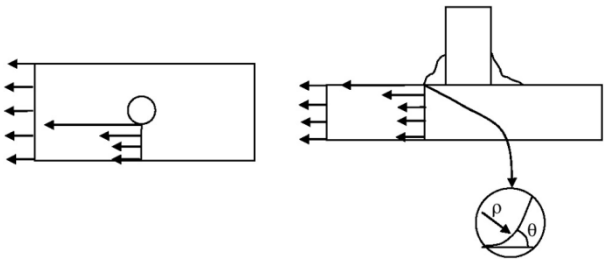

Figure 11 Notch effect at the edge of a bore hole and at the weld toe [14]

When compared with the fillet weld, the butt welded joints result fewer geometrical factors and this lowers the stress concentration with respect to the fillet joint increasing the fatigue life. However; the location where the weld metal meets the base material will still be the failure location.

As a summary any welding operation would be responsible for notch effect, micro flaws and residual stresses no matter how sensitive the operation is carried out and especially at higher loads these factors would be dominating when compared the other material properties. Also the variation of these parameters will be responsible a serious scatter in the fatigue data, hence in order to determine the fatigue life of a welded joint, a detailed and statistical fatigue test plan should be carried out since these factors cannot be idealized. [14]

CHAPTER 3

LITERATURE REVIEW

3.1 Welding Cast Iron

Pascual et al. [15] have studied welding nodular cast iron with oxyacetylene (OAW) and shielded metal arc welding (SMAW) using 98.2% Ni and Fe-Cr-Ni alloy filler materials respectively. They have concluded that welding ductile cast iron with or without preheat is possible but preheating almost always increases weld quality and ductility. OAW results very poor weld metal properties whereas SMAW yields an amount of ductility in the weld metal. Furthermore, using Ni electrodes is another factor increasing the ductility which hinders the carbide formation.

El-Banna [16] has studied welding ductile cast iron in as-cast and fully ferritized states using SMAW process with ENiFe-CI filler material. He has worked on different preheating temperatures and again concluded that ductile cast iron can successfully be welded with or without preheating using Ni based electrodes but in order to achieve certain mechanical properties a preheating temperature of 200-300°C is required. Additionally he stated that R_m values required from the base materials can only be met in ferritized components. In as-welded specimens ledeburitic carbide structures and local melting around the graphite nodules are observed. With application of preheating various pearlite and martensite ratios instead of carbide were formed.

Again in a study carried out by El-Banna et al. [17] restoration properties of pearlitic cast iron using SMAW with various filler materials as Ni, Fe-Ni alloy, Ni-Cu alloy, stainless and ferritic steel is studied. Also subcritical annealing at 677°C is applied. Effect of heat input, preheating and filler materials was examined. When using the ferritic filler material, preheating at 300°C becomes the best option for narrowing the

melt region and HAZ with discontinuous carbide and bainite. It is seen that PWHT has reduced the maximum hardness values slightly and finally multipass welding lowers the width of melt region and microhardness of HAZ. Using filler materials with Ni content can overcome carbide formation however; with ferritic filler a continuous carbide network is observed around the fusion line and HAZ yielded a martensitic structure.

Pouranvari [18] carried out a study on welding cast iron using SMAW with Ni based electrodes. He also applied PWHT to the welded pieces. Due to possibility of increasing amount and continuity of carbides preheating is not used and formation of cracks was not reported. Material was fully annealed and a nearly uniform hardness profile is achieved. Again nickel based filler is used to prevent ledeburitic carbide formation in the structure of the weld piece but due to dilution very high carbon contents are come across which cannot be compensated with Ni. This excess amount precipitated as graphite in fusion zone. In PMZ ledeburitic and martensitic structure formation occurs, constructing a hard and brittle network among fusion line.

Voigt et al. [19] have studied general HAZ structures of ductile cast irons. SMAW with ENi-CI filler material used with about 300°C of preheating. Sub-critical annealing and full annealing is applied to the specimens. In as weld specimens carbides are formed surrounding the graphite nodules and in intercellular regions between nodules. It is concluded that this formation cannot be effectively prevented in PMZ. Martensite, observed in HAZ, cannot be overcome if the preheating temperature is sustained for sufficient times after welding. By application of subcritical annealing martensite was decomposed to ferrite and secondary graphite.

3.2 Dissimilar Welding of Cast Iron

Hatate et al. [20] have made a comparison of dissimilar welding of spheroidal graphite cast iron to mild steel between electron beam welding (EBW) and MAG welding. For this purpose a buffer layer of nodular cast iron with 35% Ni was inserted between the two types of materials in EBW welding and Ni alloy filler wire is used for MAG welding. Very high cooling rates and high hardness values were experienced in weld bead of EBW joints. Increasing the objective to focus distance ratio resulted a lower cooling rate and lower hardness but increased bead width. This

modification has not affected bonding strength. Because of the lower heat input it is judged that EBW results and increased bonding strength with respect to MAG. Cementite formation in EBW welding is observed and successively prevented using Ni layer. It is seen HAZ region of cast piece in MAG welded joint is composed of cementite and martensite.

Sanghoon et al. [21] studied dissimilar weld joint between high silicon nodular cast iron and ferritic stainless steel using MAG welding with Ni Cr alloy filler material. A significant UMZ region is determined on the fusion boundary. This region with PMZ has yielded the highest hardness values and martensitic phases and carbide formation is examined in UMZ, PMZ and HAZ. Additionally in PMZ and HAZ parallel to the peak temperatures a carbon diffused layer is formed around the graphite nodules.

3.3 Partially Melted Zone of Nodular Cast Iron

Laser surface remelting was applied to the nodular cast iron in order to see the microstructural changes and their effects to the hardenability behavior. In the study carried by J. Grum and R. Sturm [22] CO_2 laser of 450 W was applied on the surface of ferritic pearlitic nodular iron. In such a case two layers are described as remelted and hardened layer. The remelted layer has similar characteristics to the fusion zone and hardened layer to the HAZ. The hardened layer transforms into austenite during heating and carbon diffuses into austenite at these increased temperatures. Formation of carbon concentration gradient at neighborhood of nodules is reported. At regions close to the graphite, the matrix carbon concentration increases reaching the values of eutectic composition. At these regions the temperature at heating becomes sufficient for melting and upon cooling ledeburite is formed. Further away from the spheroids, the carbon concentration decreases increasing the melting point of that region. This time temperature of heating becomes insufficient for melting and a martensitic shell is built surrounding the ledeburite. For graphite nodules away from the heat no melting takes place, only hard martensite forms around the nodules. This phenomenon was summarized with a very good sketch in the study, as shown in Figure 12.

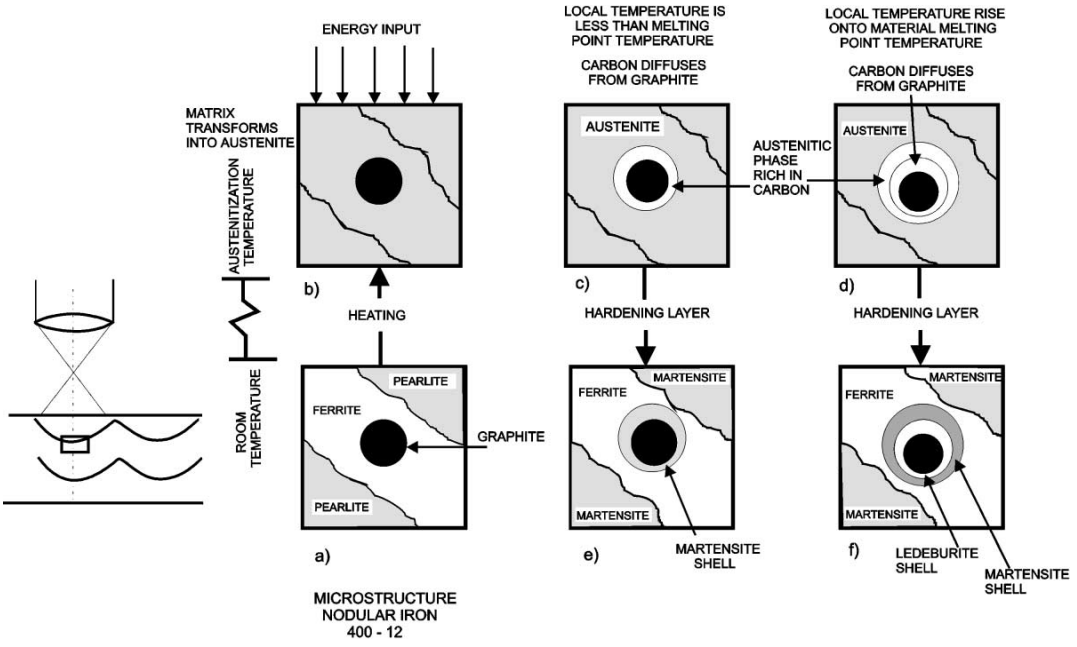

Figure 12 Formation of ledeburitic and martensitic shell around graphite nodule [22]

In another study carried out by Benyounis et al. [23] nodular cast iron surface was melted by laser beam and tungsten inert gas (TIG) arc and the solidification structures were classified and compared. In both ways, graphite was completely dissolved during melting and solidified in a dendritic manner. The dendrites have transformed to austenite in a eutectic matrix composed of austenite and iron carbide in the TIG applied specimens. Due to the lower heat input of the laser beam, upon solidification finer dendrites of retained austenite is formed. These dendrites are surrounded by iron carbide and martensite is detected in the dendrite arms. Hardness values of 750HV are reached in TIG process while laser beam yielded about 600HV.

3.4 Fatigue Behavior of Cast Iron

Very high cycle (10^{10} cycles) fatigue behavior of nodular cast iron is studied by Xue et al. [24]. Fatigue behavior and effect of frequency is not observed. Crack initiation takes place on surface graphite nodules or subsurface nodules.

Mechanisms of crack propagations of cast irons with various pearlite and ferrite ratios are investigated by Cavallini et al. [25]. Common damaging mechanism for crack propagations is determined to be the debonding of the graphite elements which is characterized by the morphology depending on microstructure. Microstructure

influences the crack propagation resistance only at higher stress ratios while at lower ones no variations can be determined. Pearlite results in a completely fragile debonding mechanism whereas ferrite yields higher ductile deformation during debonding. Pearlitic ferritic structure fractures at intermediate values. The ductile debonding mechanism acts as an important crack closure mechanism. Finally it is concluded that phase distribution in the structure, like bull's eye structures, acts as a secondary crack closure mechanism.

CHAPTER 4

EXPERIMENTAL PROCEDURE

The experimental procedure consists of material selection, their characterization, welding and parameter optimization and finally mechanical property determination steps. First of all, two types of materials suitable for the project were selected. The chemical and mechanical properties and their behavior under welding were examined. Suitable parameters for both materials were decided according to these behaviors. Using these parameters the materials were joined, then variations of hardness and microstructures according to the post weld heat treatments were classified. For further mechanical classification of the joint, tensile and impact toughness tests, were applied and tensile fatigue behavior was characterized. In order to determine the cracking mechanism, fractography studies were carried out. A general flow chart summarizing the experimental procedure is drawn in Figure 13.

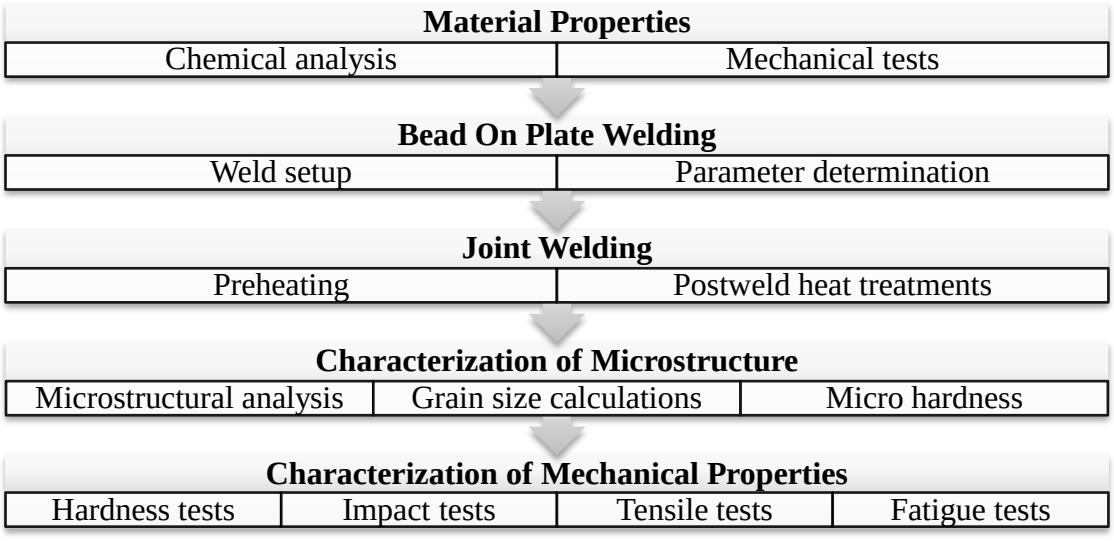

Figure 13 Experimental procedure flow chart

4.1 Materials Used

Two types of materials have been chosen in order to represent the two material types as ductile cast iron and low carbon steel which are GJS600-3 (classified according to EN 1563 [26]) and E355 (classified according to EN 10297-1 [27]) respectively. These two materials were joined using G3Si1 (classified according to ISO 14341 [28]) filler wire. The chemical compositions of these materials are given in Table 1. Composition of E355 was obtained by spectral analysis and the data of the filler wire was directly taken from the manufacturer website [29]. GJS600-3 was cast by Akdaş Casting Ind. Trade Co. and its composition was provided upon delivery of the material. The mechanical properties of the materials can also be seen in Table 2. GJS600-3 and E355 base metals were tested and properties of G3Si1 were again taken from the manufacturer.

Table 1 Chemical compositions of the materials (wt%)

Materials	C	Mn	P	Si	S	Cr	Cu	Mg	Mo	Ni
E355	0.07	0.92	0.04	0.08	0.01	0.18	0.02	-	0.03	0.25
GJS600-3	3.6	0.4	0.03	2.30	0.002	0.05	0.4	0.05	0.05	0.08
G3Si1[29]	0.08	1.50	-	0.85	-	-	-	-	-	-

Table 2 Mechanical properties of the materials

Materials	R_e, $R_{p0.2}$ (MPa)	R_m (MPa)	Elongation (%)
E355	415	515	28
GJS600-3	405	605	3.8
G3Si1	440	540	30

The microstructures of the base metals were examined and taken into account to be used as the reference state for comparison to the states after welding and heat treatments.

4.2 Weld Setup

Weld setup mainly consists of two main parts. The first one is the wire feeder integrated power source and the second one is welding truck which was used to stabilize the welding speed throughout the welding process.

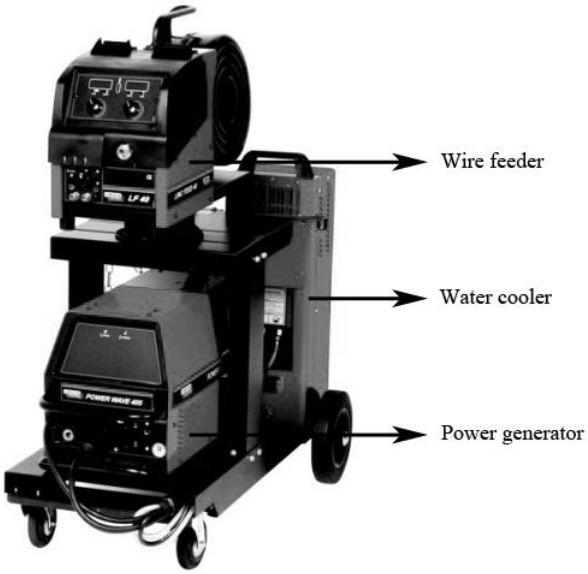

Figure 14 Lincoln welding machine, with power generator, wire feeder and water cooler

As the welding machine a system combined of Lincoln Power Wave 405m power generator, Lincoln Line Feed 40 wire feeder and water cooler (Figure 14) was used. The wire feeder was installed with the console (Figure 15) enabling setting up of welding parameters and weld programs according to the materials used and type of welding.

To adjust the desired welding speed and neglect the variations caused by manual welding; Messer Griesheim Quicky E Flame Cutter was used as a weld truck (Figure 16). The numbers shown on the speed knob do not correspond directly to welding speed in known units. Hence the speed of the truck (in mm/sec) corresponding to the scale on the knob was measured and listed in Table 3.

Table 3. Welding speeds corresponding to welding truck

Knob	1	2	3	4	5	6	7	8	9	10
Speed (mm/s)	1.37	4.05	6.58	8.55	10.75	12.35	14.08	15.15	16.95	17.86

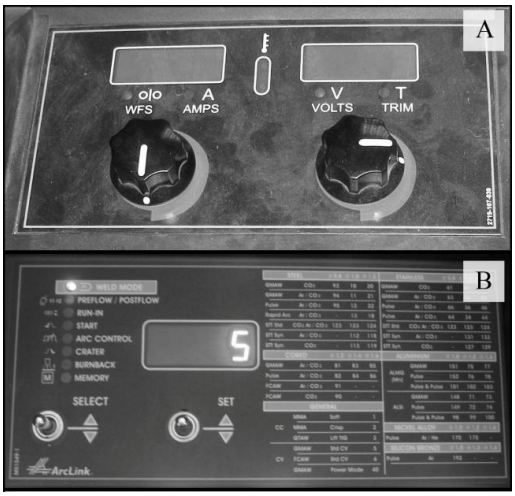

Figure 15. Setup console installed on the cover of wire feeder (A. Outside, B. Inside)

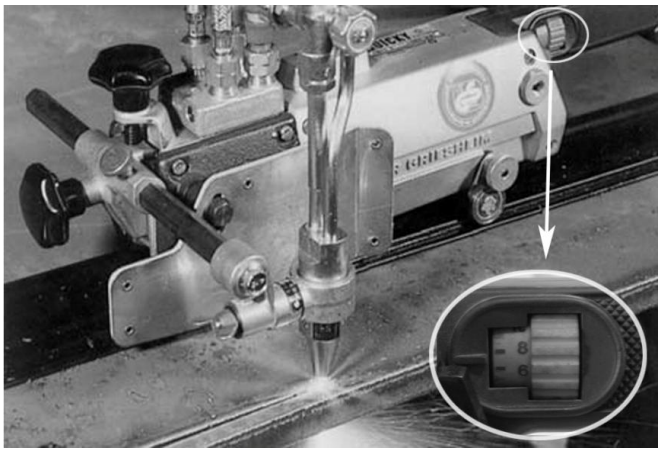

Figure 16 Messer Griesheim Quicky E Flame Cutter. Speed knob is showed in a magnified scale.

4.3 Bead on plate weld tests

Bead on plate welding is a method to determine the behavior of the materials under weld operations. This method, in which a single bead of welding is applied over the

base material, does not include a joining operation. Main purpose of this method is to get to know the material used better and determination of the suitable welding parameters for the chosen material.

For test, plates having dimensions of 5x50x100mm were used. Bead on plate welds were done using constant voltage (30V) and weld speed (15.15mm/s). The wire feed speed (WFS) and hence current of the weld was modified in order to see the change in penetration. Although the welding voltage and WFS were set to constant values, due to the fluctuations on current and voltage values during welding, at the end of each weld pass the average welding parameters during that pass was obtained from the power supply and recorded. Table 4 shows these parameters.

Table 4 Bead on plate welding parameters with constant welding speed (15.15mm/s)

E355		**WFS (m/min)**	**GJS600-3**	
Voltage (V)	**Current (A)**		**Current (A)**	**Voltage (V)**
25.9	292	9.49	272	25.8
26.5	316	10.00	302	26.6
27.3	331	10.51	262	26.6
29.4	359	10.99	291	28.3
29.0	374	11.50	319	28.6
29.0	385	12.01	344	29.6
28.5	377	12.49	314	28.3

First thing to take into consideration determining the suitable welding parameters was the penetration depth of the weld. In bead on plate weld tests parameters giving out the similar penetration depths for E355 and GJS600-3 were tried to be determined. In order to see the effects of the welding parameters, the materials were cut from the middle length and the cross-section was examined in macro scale.

4.4 Joint welds and preheating and post weld heat treatment (PWHT)

For joining of the materials, butt welding of plates having the dimensions of 5x50x100 mm was planned. As seen in Figure 17 the edges were beveled obtaining a V shape having an angle (θ) between 30 to 45°. The plates were placed having a separation equal to the filler wire diameter (d = 1.2mm) and backing of E355 steel with 5mm thickness was used.

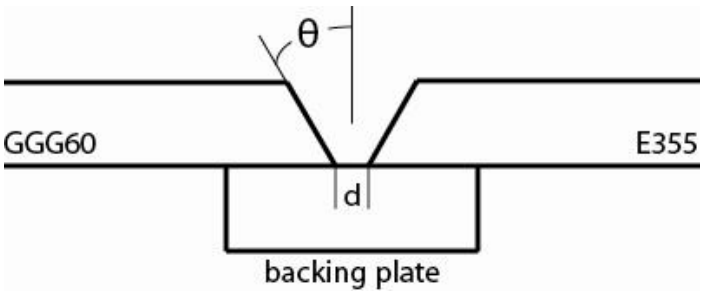

Figure 17 Weld geometry

In order to prevent the crack formation upon cooling, the base materials were preheated before processing the welding. Above explained welding geometry was constructed and the materials were fastened by weld spots. The fastened work piece was heated in furnace at 350°C.

The joining operation was carried out in two steps for the above explained welding geometry. Hence, parameters obtained by the bead on plate welds were modified suitably for penetration depths required of two passes and slower welding speeds. The joint was completed in two successive passes without allowing cooling of the weld zone between them. When welding was completed, materials were cooled in open air.

In order to modify the hardness of the weld plates, PWHT was applied. The specimens were placed into the previously heated furnace at 400°C and 700°C and held inside for 1.5 hours and cooled in the furnace with a cooling rate changing between 1.5°C/min and 1°C/min (Figure 18).

4.5 Mechanical Tests

To see the effect of the applied heat treatments on the mechanical properties, weld pieces were subjected to hardness, tensile, charpy-impact and fatigue tests. Three groups of metals were used as as-weld (AW), heat treated at 400°C (PWHT400) and heat treated at 700°C (PWHT700).

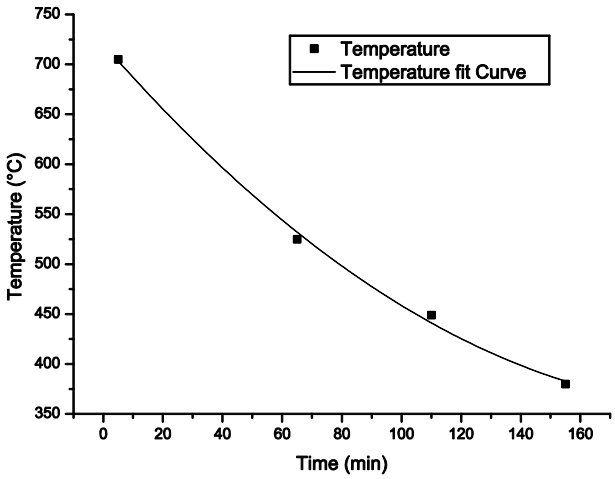

Figure 18. Cooling curve of the heat treatment furnace

4.5.1 Hardness Tests

Hardness tests were applied to the heat treated and as-weld metals in order to determine the change of hardness distribution over the cross-section with respect to the applied PWHT. The welded plates were cut from the middle of the weld seam, grinded up to 800 grit and hardness values were measured according to EN 1043-1 [30] standard. According to this standard, Vickers hardness measurements were taken from the base metals, heat affected zones (HAZ), fusion lines for GJS600-3 and E355 material sides and from the weld metal itself (Figure 19). Three measurements each for base metals, weld metal and fusion lines, 2 measurements for HAZs were taken from two mm below the upper surface. Measurements for fusion lines were taken just inside the HAZ at the weld metal side, along the fusion line. For hardness indentations Shimadzu HSV 20 Hardness tester was used. 10kg of load was applied to the specimens for 15seconds.

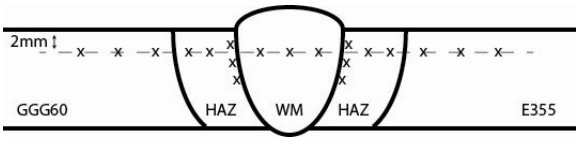

Figure 19. Locations of the hardness indentations on a joint weld cross-section

Micro hardness tests were applied in order to determine the hardness values of different phases and zones formed during the welding. For micro-hardness tests Shimadzu HMV-2 Micro Hardness Tester was used. 200gr is applied to the specimens for 10 seconds.

4.5.2 Tensile Tests

Tensile tests were applied in order to determine the mechanical characteristics of E355 and GJS600-3 and weld pieces. For E355 steel 20x10mm cross-sectioned specimens having gage lengths about 80mm, for GJS600-3 20x10mm cross-sectioned specimens having gage lengths about 100mm were prepared. Welded specimens prepared in much smaller fashion for specimen preparation issues. These specimens had 4-5x6-8mm cross sections and about 45mm of gage lengths Figure 20 and these specimens were tested at room temperature according to EN 895 [31] international standard and the stress strain behaviors were determined.

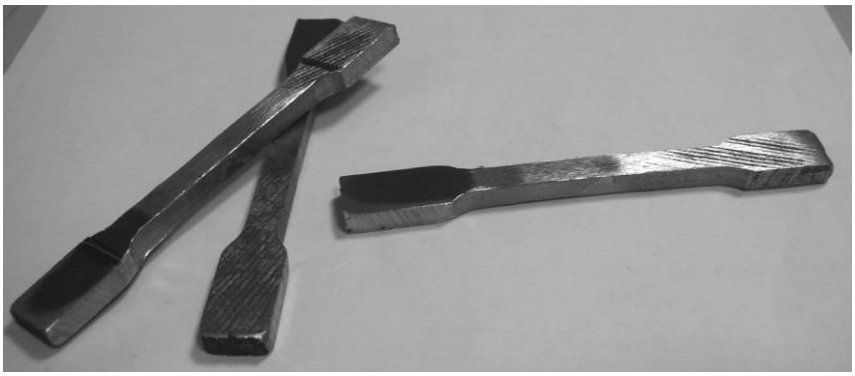

Figure 20 Tension test specimens

For base material tests ALŞA Universal Hydraulic Tensile Testing Machine having 40tonnes capacity was used and welded materials are tested by Instron 5582 Electromechanical Tension Tester. Stroke controlled strain measurements were carried out, and elongation percents are calculated by measuring the initial and final gage lengths.

4.5.3 Charpy-Impact Tests

Weld pieces were tested according to EN 875 [32]. Three sets of impact specimens for each heat treatment method and as weld state were prepared. The specimen dimensions are shown on Figure 21.

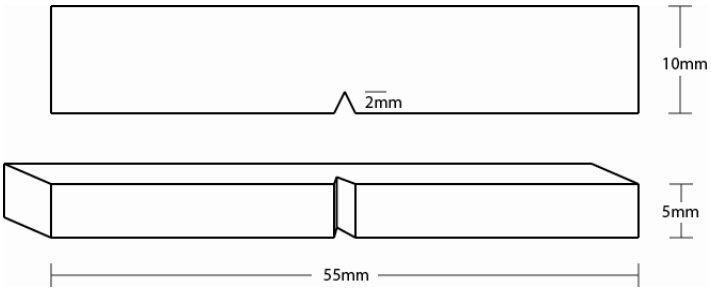

Figure 21 Impact toughness specimen dimensions

For three different heat treatment groups the impact properties of weld metal and fusion lines of both cast iron and steel sides were examined. For this purpose 2mm of V notches were introduced to the fusion lines and weld metals. The locations of the notches can be seen in Figure 22. The tests were carried out at room temperature using Zwick Roell Pendulum Impact Tester of 300J capacity.

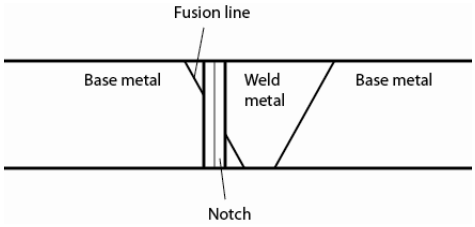

Figure 22 Notch location of an impact toughness specimen

4.5.4 Fatigue Tests

To determine behavior under dynamic loading conditions the weld plates were tested applying constant amplitude tensile stress between 0 and 350MPa at 5Hz frequency

using Dartec 9500 Universal Testing System. The test was applied to the as-weld and PWHT plates. The specimens were tested until fracture occurred and cycle count and fracture locations were recorded.

4.6 Mechanical Test Specimen Preparation

All the mechanical test specimens were prepared in the same fashion. When the weld piece was prepared the backing was removed and the root and face of the welds were ground (Figure 23). The first and the last 15mm of the plates were removed to discard possible welding faults at the beginning and the end, then strips having 15mm width were produced (Figure 24), these strips were finally machined to have the desired test piece shapes shown on above images. The heat treatments were applied after the final shaping operation.

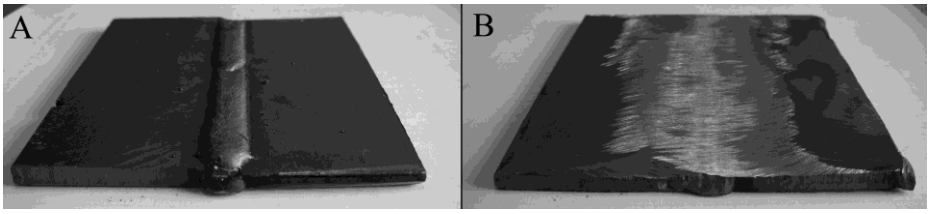

Figure 23 Welded plates. A. as-weld, B. tip and root of the weld are ground

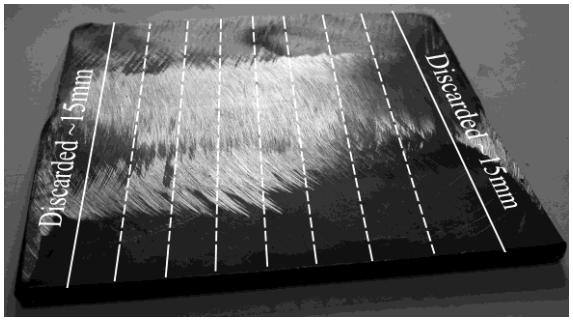

Figure 24 Strips to be removed and discarded pieces are schematically shown

4.7 Macro and Micro Examination

The entire bead on plate, joint weld and dynamic load test specimens were examined in macro scale in order to see the penetration of the weld and possible weld

discontinuities along the cross-section. For macro preparations the specimen surface to be examined was grinded for sufficient grades. The photographs of the specimens were taken using a computer scanner at 600 dpi quality.

Micro examination was used for examining the micro-structure of the joint and the change in the phases present with the effect of heat treatments. Also the fracture surfaces of the fatigue tests were examined in order to determine the fracture characteristics of the weld pieces. For these processes scanning electron microscopy in addition to the regular micro examination methods were used.

4.8 Grain Size Measurement

Grain size determination was carried according to ASTM E 112 [33] using the Heyn Lineal Intercept Procedure. Images for grain size calculations were taken from three different weld plates for each heat treatment state (as-weld and tempered at two temperatures). Calculations were done in x, y and z axis for all images. Lines longer than 600µ were drawn on these directions as shown in Figure 25 and total number of interceptions was counted. Dividing the total length to intercept count, average intercept lengths were calculated in determined directions. Total number of 12 calculations were done for as-weld and tempered states. Using *Table 6* and *Table 4* on ASTM E 112, ASTM Grain Size Numbers (G) and average grain diameters were determined.

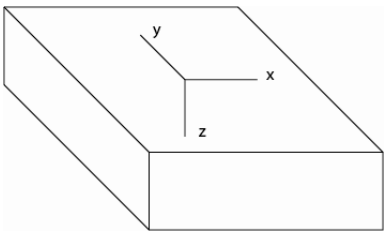

Figure 25. Grain size measurement directions

CHAPTER 5

RESULTS AND DISCUSSION

In order to characterize the base materials, micro examinations, hardness and tensile tests of GJS600-3 and E355 were carried out. These steps were taken in order to compare the material properties before and after the welding and heat treatment operations. To further see the base metals' behavior under welding, bead on plate welding examinations were performed and suitable welding parameters were determined for joining operations. For preventing possible weld cracks that may occur, suitable preheating temperature was determined. By combination of these parameters and preheating, successful weld joints were constituted. By micro examinations the general characteristics of the microstructure, by hardness, tensile, impact and fatigue tests mechanical properties of the weld joints are determined. Finally effect of heat treatments temperature on all these properties was classified.

5.1 Discussion about the Base and the Filler Metals

In the joining operation the main properties of the materials determine the main characteristics of the welded piece. Hence a comparison between the properties of the materials was carried out.

5.1.1 Filler Wire Selection

The construction in subject to this study was aimed to bear static and dynamic loads. For this case cold welding with Ni fillers was not considered. Selection of a filler primarily suitable for E355 was chosen for its superior mechanical properties. Therefore it was determined to work with G3Si1.

5.1.2 Chemical Composition

The chemical compositions of the materials used in the welding process are listed in Table 1. E355 has a low carbon composition. G3Si1 filler wire has equivalent carbon content to E355 and has similar alloying element concentration values. GJS600-3 shows quite different chemical composition with various other elements that are not present in E355 which are characteristic to nodular cast irons. The most important factor related to welding is the high carbon content of the cast iron. High amount of carbon with combination of other elements increase the CE of cast iron and decrease the weldability. The lower weldability of cast iron can require preheating and post-weld heat treatment to achieve desired properties. If the heat introduced during these operations is not controlled well, this may lead spoiling the main structure of E355 base material and it is not in any case tolerable to degenerate the base material properties during the welding operation. So, minimum damage, if possible none at all, should be caused to the steel piece.

Additionally, because of the difference in chemical compositions, dissimilar welding features were also introduced to the subject. These features require a more careful welding operation. In this case dissimilar melting points are the most important fact to be taken into consideration related to the dissimilar welding. Higher heat requirements of E355 cause more than enough heat to be transferred to GJS600-3 and this causes formation of undesired melted regions of the cast piece. These will be covered in micro examination section.

5.1.3 Tensile Properties

Mechanical properties of the materials are shown in Table 2. Here, the most important difference was seen in the elongation. The steel has the capability to elongate more than 7 times as the cast iron and GJS600-3 shows lower yield and higher tensile strengths than E355. The material failure of GJS600-3 in tension would lack the toughness with its 3.8% elongation. In tensile loading composed of these three constituents, assuming the structures are preserved and no flaws are created during welding, the first material to yield would be GJS600-3 followed by E355 and the filler material respectively. As the load is increased, when 515MPa is reached, the necking will begin at E355 side and the weld joint would fail from that

region. Although GJS600-3 yields first, steel piece and filler material will elongate before failure and in such a case, a successful joint between these materials will provide some elongation. This will be advantageous when compared to a single cast piece loaded in tension.

5.1.4 Microstructures

The images taken from the base materials can be seen in Figure 26 and Figure 27 for E355 and GJS600-3 respectively at different magnifications. E355 has a ferritic matrix. In addition, some amount of pearlite can be seen in the microstructure as well. Grain boundaries are clearly visible and a grain orientation caused during formation is detectable. The microstructure of the GJS600-3 consists of graphite nodules distributed in pearlitic matrix. The graphite nodules are surrounded by ferrite constructing the bull's-eye structure.

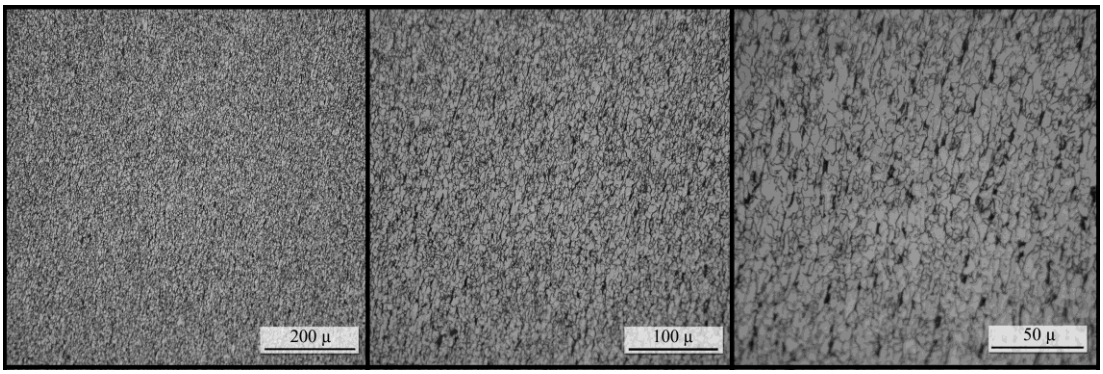

Figure 26 Microstructure of E355 steel in different magnifications.

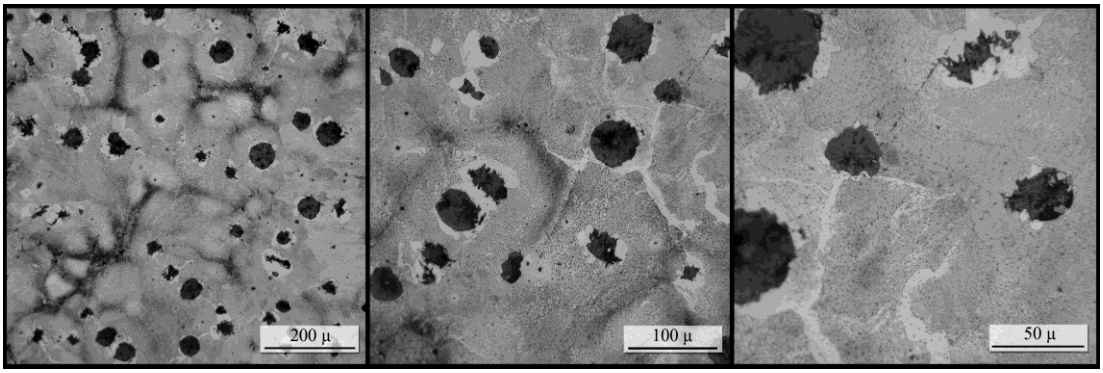

Figure 27 Microstructure of GJS600-3 cast iron in different magnification

Upon joining, the filler material will act as an intermediate medium in between two materials. The E355 fusion site was not expected to cause any problems because of the similar structure of filler and the steel. But in cast side it was a great possibility to come across very different microstructures in a joint of ferritic steel piece to pearlitic nodular cast iron. The combination of high cooling rates with the dissimilar welding characteristics would cause undesired microstructures to be created.

5.2 Bead On Plate Weld Examinations

Measuring the penetration depths with respect to varying weld parameters, suitable parameters for joining operations were determined. In Figure 28 a representative macro photograph of the bead on plate welding specimen is shown. Using macro examination of the specimens, penetration percent of the respective welding parameters tried to be figured out.

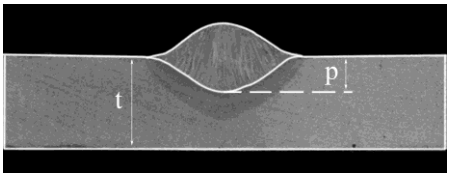

Figure 28 Macro photograph of a bead on plate weld specimen (p: penetration depth, t: material thickness)

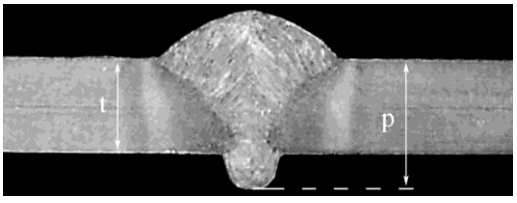

Figure 29 Pierced bead on plate weld specimen (p: penetration depth, t: material thickness)

Penetration percent was calculated by dividing the penetration depth to 5mm thickness of the materials. The respective penetration depths of the parameters were

tabulated in Table 5. This table was constructed with constant welding speed of 15.15mm/s. Penetration percents higher than 100 means that the weld piece is pierced due to the increased parameters and a root having significant height is constructed on the other side of the specimen (Figure 29).

Table 5 Variations of weld parameters and penetration depths with respect to increasing WFS at constant weld speed.

E355			WFS (m/min)	GJS600-3		
Penetration Percent	Penetration (mm)	Current (A)		Current (A)	Penetration (mm)	Penetration Percent
50	2.5	292	9.49	272	2.5	50
64	3.2	316	10.00	302	2.4	48
66	3.3	331	10.51	262	2.1	42
84	4.2	359	10.99	291	2.7	54
76	3.8	374	11.50	319	3.2	64
110	5.5	385	12.01	344	5.0	100
140	7.0	377	12.49	356	5.6	112

The penetration affinities of the materials are graphically shown on Figure 30. It was determined to complete the welding operation in two passes in order to lower the heat input in single step. For such operation, considering the weld groove, weld penetration sufficient for the half of the weld plate or less was considered to be sufficient. Hence parameters yielding 45-55% penetration is taken as basis for joint operations.

5.3 Joint Weld

When joining the two metals together certain welding properties were aimed. These were:

a. suitable penetration for two material types,
b. a joint without any discontinuities,
c. homogeneous hardness distribution.

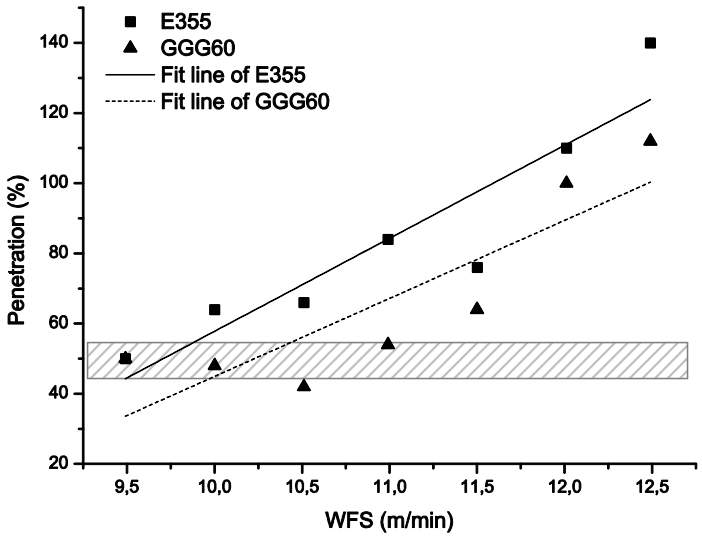

Figure 30 Penetration affinities of the materials with respect to WFS. The penetration requirement for welding operation in two passes is shown with the shaded rectangle.

For a suitable weld root joint with sufficient penetration, the weld speed was lowered. A modification of parameters was applied considering the energy input of the single weld pass. To prevent crack formation preheating and to homogenize hardness values post weld heat treatments were applied. Hardness was studied as the basis of the mechanical properties for two main reasons; firstly it can be a reflection of brittleness and secondly it can be measured easily through all weld cross section. All these studies were supported by micro and macro examinations and hardness testing.

5.3.1 Parameter Modification

In order to be able to achieve a successful root joint, the weld speed was lowered to about half of the one that was used for bead on plate weldments. WFS was reduced proportionally to weld speed to have similar penetration values. Reducing WFS also lowers the metal deposit amount and leaves free space in the groove for additional weld passes. Voltage was also reduced to provide required penetration. With

application of several passes, new values of 4.80 m/min, 6.58 mm/s, 20V are set for WFS, weld speed and voltage respectively.

Heat input calculations were carried to see that the parameter changes were done in an acceptable frame. For this purpose line energy equation:

$$Q = k\frac{UxI}{v}x10^{-3} \text{ kJ/mm (2),}$$

was used. When inserted into the equation the bead on plate parameters yielding 50% penetration gives 0.370 kJ/mm and 0.399 kJ/mm respectively for GJS600-3 and E355 and modified parameters yield 0.433 kJ/mm heat input. The newly determined parameters were used for both passes and were tabulated in Table 6.

Table 6 Joint weld parameters

	WFS (m/min)	**Voltage (V)**	**Weld Speed (mm/sec)**	**Current (A)**
Pass 1 & 2	4.75-4.85	18-22	6.40-6.60	120-140

5.3.2 Preheating

When examined in macro scales cold cracks was observed on the joint weld specimens especially at the root of the joint (Figure 31).

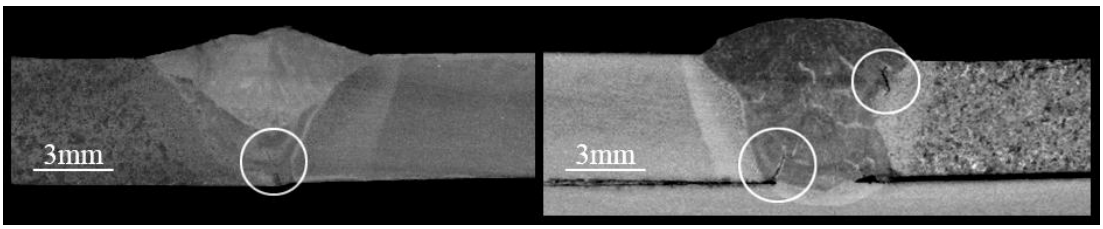

Figure 31 Macro photographs of the weld cross-sections. Cooling cracks are shown.

Combination of high cooling rates of welding with increased carbon content of cast piece causes massive martensite formation in very short times. This transformation results formation of cracks at the last stages of welding. Cracks formed in the martensitic weld metal can be seen in Figure 32.

Determination of preheating temperature was done with respect to the CE of cast piece. When calculation was carried out according to the theoretical chemical composition of the GJS600-3 given in the Table 2, the equation gives out the carbon equivalent of GJS600-3 as 4.53. When inserted into Figure 9 this value shows no-crack preheat temperature range between 250 to 320°C. And it is also reported that selecting preheating temperatures higher than 315°C minimizes martensite formation, residual stresses due to welding and possibility of crack formation [8]. In light of these information, minimal applicable preheat temperature was selected to be 350°C for joint welds and it was seen that formation of cooling cracks successfully prevented.

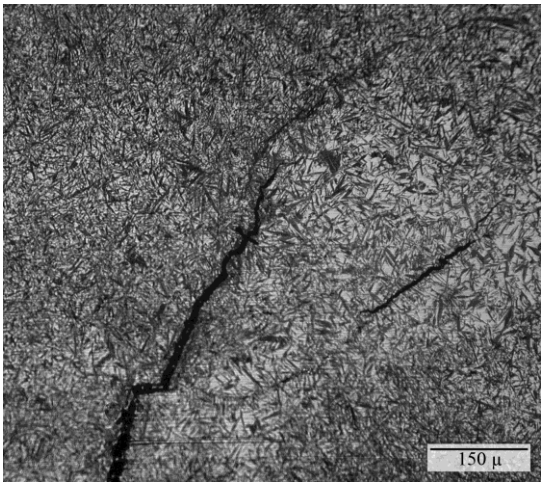

Figure 32 Cracks formed in the weld metal on the regions near to the root of the weld

5.3.3 Post Weld Heat Treatment (PWHT)

PWHT was carried out primarily to see the effect of heat treatment on the general properties of the welded joints. The purpose was to modify the microstructure and to

examine the effect of this modification over the general mechanical properties of the joints.

Specimens were held at 400 (tempering) and 700°C (subcritical annealing) in the furnace for 90 minutes and furnace cooled. This is done in order especially to modify the martensitic structure. Heat treatments above eutectoid (fully annealing) were not applied not to disrupt the characteristic microstructures of the base materials. As expected, a great micro-structural change of the materials were examined when specimens were subjected to temperatures over eutectoid temperature and cooled slowly. After application of heat treatment at 800°C it was seen that the grain size of E355 was increased greatly (Figure 33-A). Microstructure of GJS600-3 is completely transformed into ferrite with graphite nodules and grains even larger than E355 were observed (Figure 33-B).

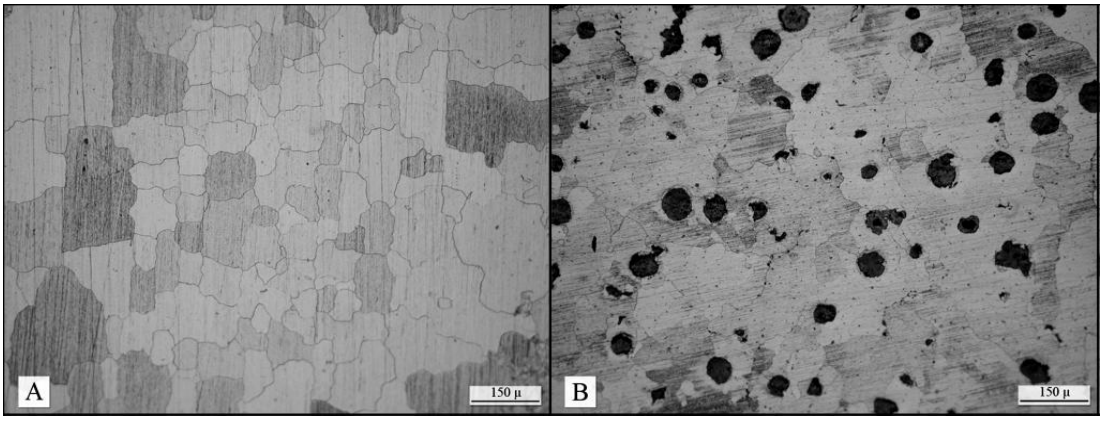

Figure 33 Micro images of the specimens heat treated at 800°C A) E355, fully ferritic microstructure with increased grain size; B) GJS600-3, ferritized, grains are visible

5.4 Micro Examination

Weld joint has been separated into two regions for micro-structural examination as E355 and GJS600-3 base metals. A more detailed study was carried on GJS600-3 site because of its problematic nature and dissimilar weld characteristics were expected to be seen in that side. The examination of E355 is mainly done to see the

possible modifications on the grain structure and this examination is supported by grain size measurements. The two base metal regions were examined in their as weld and heat treated states in order to see the effect of welding to the base materials and to examine the micro-structural changes under heat treatments. Inspections were done between fusion line and to the regions unaffected from the weld through HAZ. To support the characterization of cast iron micro hardness examination was also applied. No special study was carried on weld metal because no unusual weld metal characteristics were examined in that region.

5.4.1 E355

After welding, E355 shows a non-problematic weld structure. It was not expected to encounter any problems related to this site. It is unavoidable to break down the grain characteristics in the HAZ in any kind of fusion welding of steels however; it is always a possibility to dissipate the general grain structure of the base metal by the effect of heat treatments after welding. The microstructural study of E355 was carried mainly to see how the general structure was affected by the heat applications.

5.4.1.1 Base Metal

The base metal grain structure of the E355 was shown in Figure 34,Figure 35 and Figure 36. It was seen that the original grain form does not vary by the heat treatment. Although the main characteristics of the grain structure seem to be conserved after the heat treatments, grain size measurement was done to certainly determine possible grain size changes. Measurement data for grain size calculations are tabulated in Tables A1, A2 and A3 in Appendix A. The mean values of the average intercept lengths were calculated. Using *Table 6* of ASTM E 112 [33], ASTM Grain Size Numbers (G) were calculated. These values are listed in Table 7.

Table 7 ASTM Grain Size Numbers (G) and respective average grain diameters (d) for as-weld and tempered states.

Specimen	G	d (μ)
As-Weld	11.71	6.24
Tempered at 400°C	11.78	6.08
Tempered at 700°C	11.47	6.77

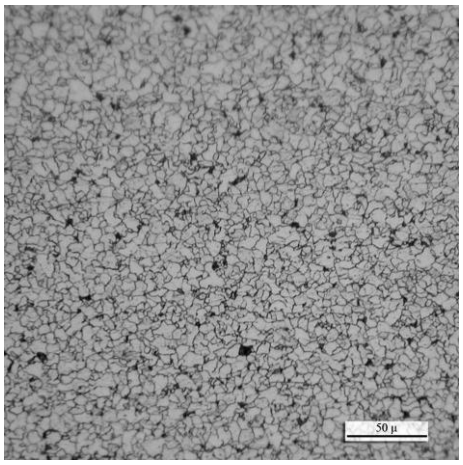

Figure 34 Microstructure of E355 base metal in as-weld state.

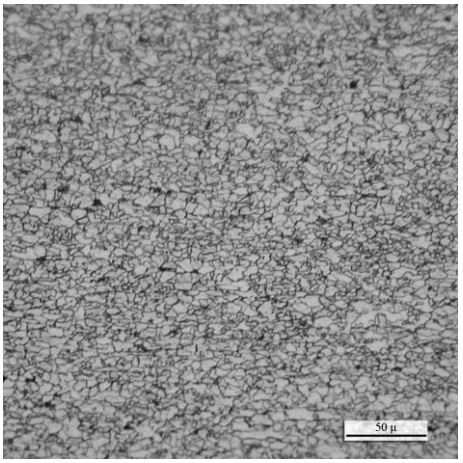

Figure 35 Microstructure of E355 base metal tempered at 400°C.

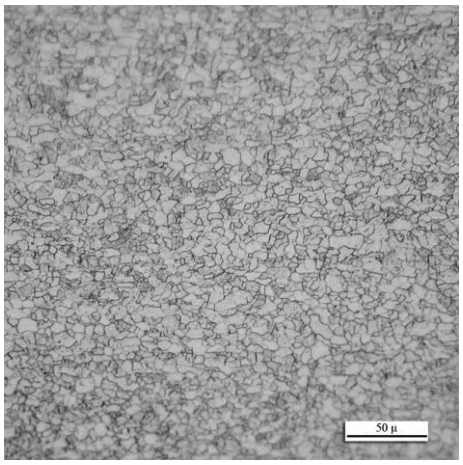

Figure 36 Microstructure of E355 base metal tempered at 700°C.

In Table 7 it is seen that average grain size of the specimens tempered at 400°C are 0.16 microns lower than the as-weld specimens. This small difference can be judged to be a result of measurement errors or image locations. However, when the grain size values of the specimens tempered at 700°C compared, it was seen that the average size of the grains was increased about 0.53-0.69 microns. Although tempering at 400°C does not affect the grain size significantly, 700°C can be responsible for an increase about 0.5 microns in grain size.

5.4.1.2 HAZ

The microstructure of the HAZ shows very different characteristics when compared with the base metal. Getting away from the fusion line, the peak temperatures, temperature gradients and thus cooling rates get lower. These changes result formation of various structures. It was observed that tempering does not cause a distinctive change in HAZ microstructure. Because of this reason, a general characterization was carried out for as-weld and heat treated states.

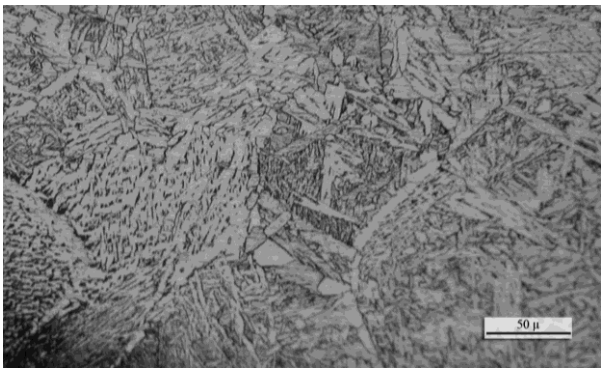

Figure 37 Microstructure of HAZ near the fusion line. The darker region on the lower left corner is the fusion line.

Figure 37 is an image taken at a location very close to the fusion line. The ferritic structure was preserved however; the general grain structure of E355 was affected in a great extend. The grains were not, in any case, in an order here. Further away from the fusion line, the grain structure was broken down at lower degrees, still losing the original base material characteristics. And as going further away from the fusion line,

the grains get a more regular structure. This change in microstructure is shown further by Figure 38 and Figure 39.

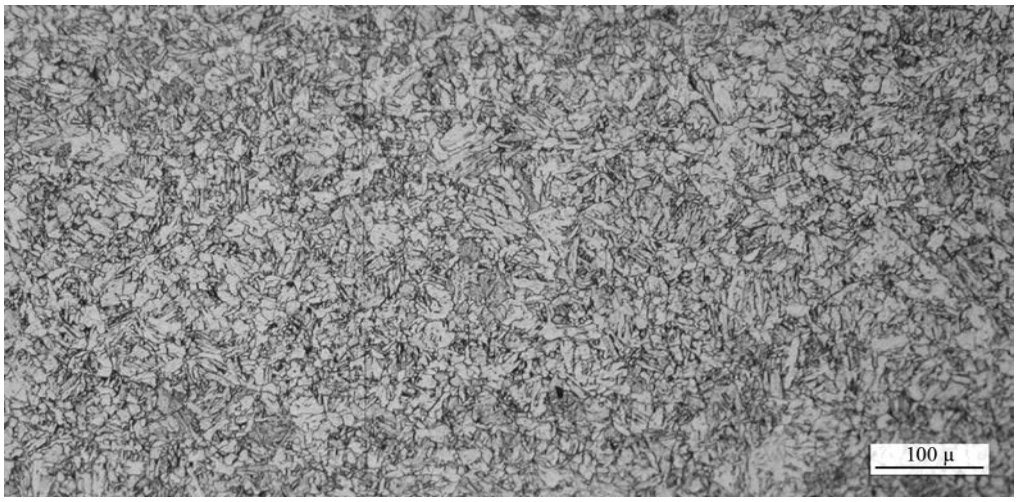

Figure 38 Microstructure of HAZ (about mid-point)

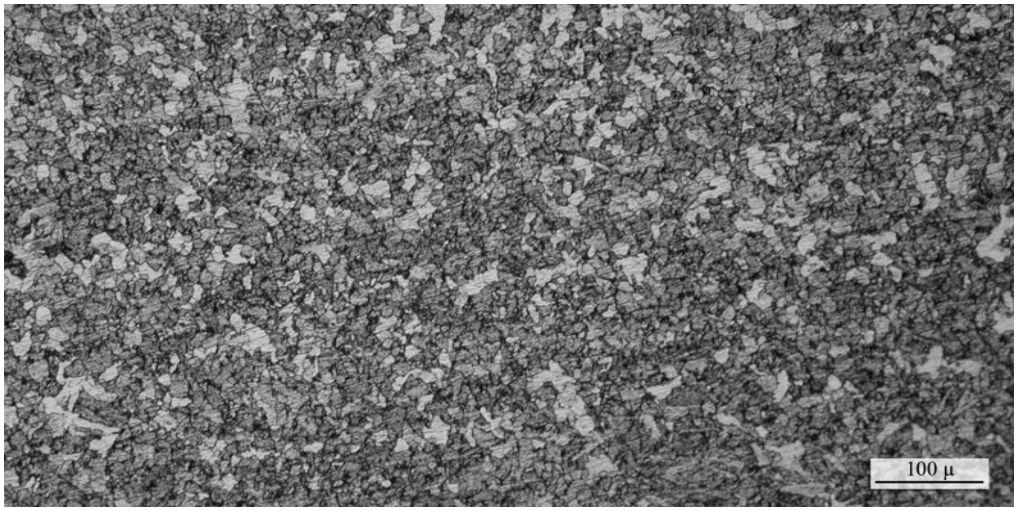

Figure 39 Microstructure of HAZ (near base metal)

5.4.2 GJS600-3

For GJS600-3, mainly because of its higher carbon content, cooling rates and post weld heat treatments become the vital steps for the successful joints. Because of the problematic characteristics, the weld parameters and pre and post weld operations

were organized with respect to this component. General properties under the effect of welding and heat treatments were tried to be sketched by microstructural examination and additionally hardness values of the phases was measured to support the characterization.

5.4.2.1 Base Metal

Base metal structure of the cast piece was not altered by the heat treatments. The general ferritic-pearlitic bull's eye structure shown in Figure 27, did not show a significant change that may be observed.

5.4.2.2 HAZ and Fusion Zone

The dissimilar welding features results formation of large melted zones in HAZ contrary to normal welding operations. The regions neighboring the fusion line melts because of the lower melting point of the cast piece and this melted region remains unmixed with the weld bath constructing the unmixed zone. A characteristic view of the GJS600-3 fusion line can be seen in Figure 40 and more detailed in Figure 41. Three distinct regions in HAZ can be determined as UMZ (unmixed zone), PMZ (partially melted zone) and true-HAZ (Figure 40). In UMZ and PMZ melting occurs but in HAZ only phase transformations take place. From now on true-HAZ will just be referred as HAZ.

5.4.2.2.1 UMZ

UMZ region is completely melted region but, mixing of filler and base metal melts cannot be achieved and the composition of this zone is accepted to be same as the base material. After welding, due to increased cooling rates, the formation of austenite at the first solidified solid occurs in a dendritic manner. When eutectoid is reached, due to fast cooling, carbon in liquid cannot precipitate as graphite and gets trapped in iron carbide. Under eutectic, cementite in combination with secondary austenite starts to form in ledeburitic structure. Further cooling below eutectoid temperatures causes transformation of austenite to pearlite or martensite according to the cooling rates.

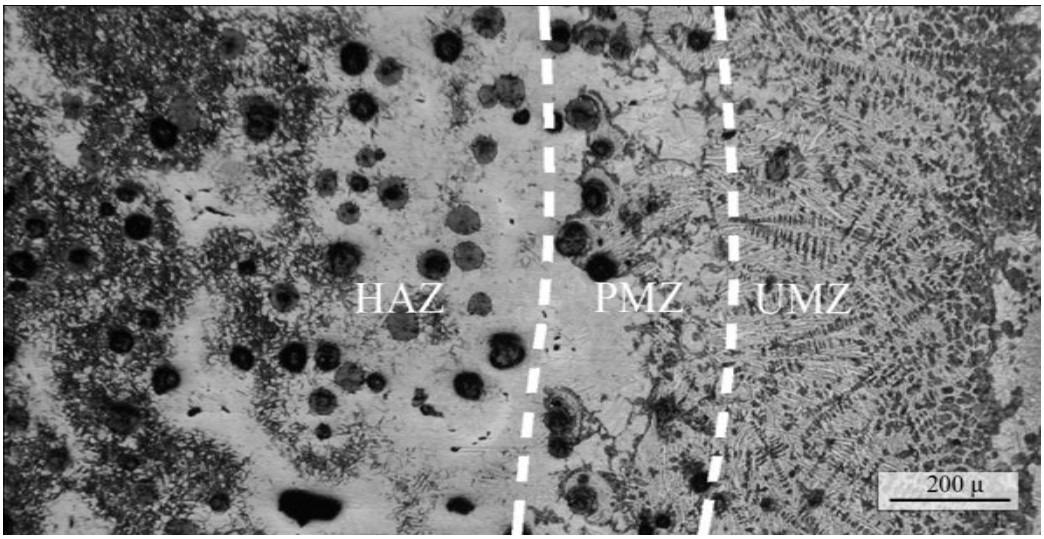

Figure 40 Fusion line microstructure of GJS600-3 (as-weld). UMZ, PMZ and HAZ boundaries are shown

During welding, UMZ having width of 300-400µ, was formed (Figure 40). In greater magnifications (Figure 41 and Figure 42) the dendrites and details of the interdendritic structure can be determined. Figure 42 shows the ledeburitic carbide formation among the dendrites. The white regions are carbide platelets among the gray martensite. A characteristic ledeburitic structure was also marked in the same figure. Additionally although cannot be detected in the etched specimens, formation of free graphite with irregular shapes and much smaller sizes than the graphite nodules could be examined in unetched ones (Figure 43). As an overall investigation, white cast iron with ledeburitic carbides among the martensitic dendrite arms and precipitated graphite construct the main microstructure of UMZ in as-weld condition.

The behavior of UMZ under heat treatments was examined. At 400°C no distinct change could be determined (Figure 44). But, when compared to Figure 44, some serious changes could be noticed in UMZ heat treated at 700°C. As seen in Figure 45, an increase in the size of the graphite precipitates and large ferritic regions were noticed. Partially decomposition of the carbides and diffusion of carbon into already present graphite allows such a behavior. Also by the effect of heat martensite was tempered, forming ferrite and pearlite.

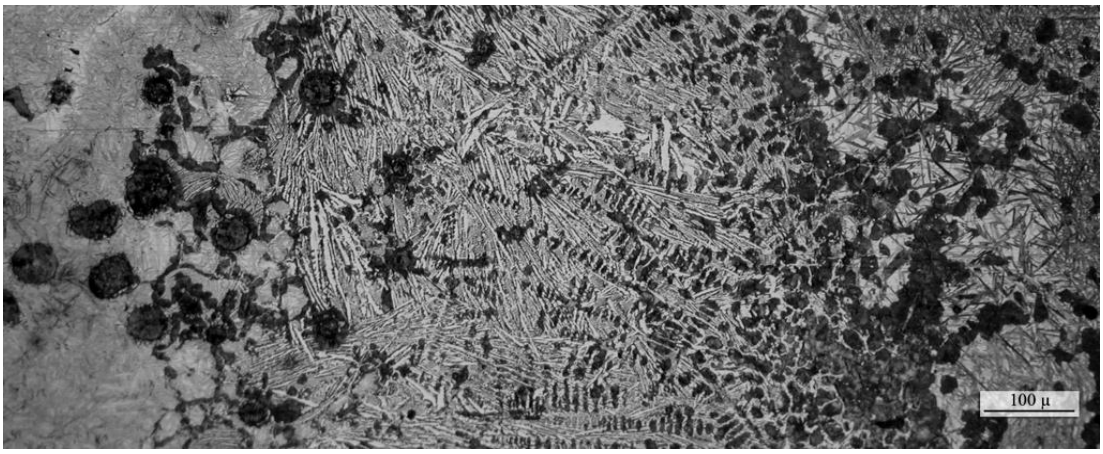

Figure 41 Fusion line microstructure of GJS600-3 (as-weld). Region between fusion line (right) and HAZ (left) is shown in more detail.

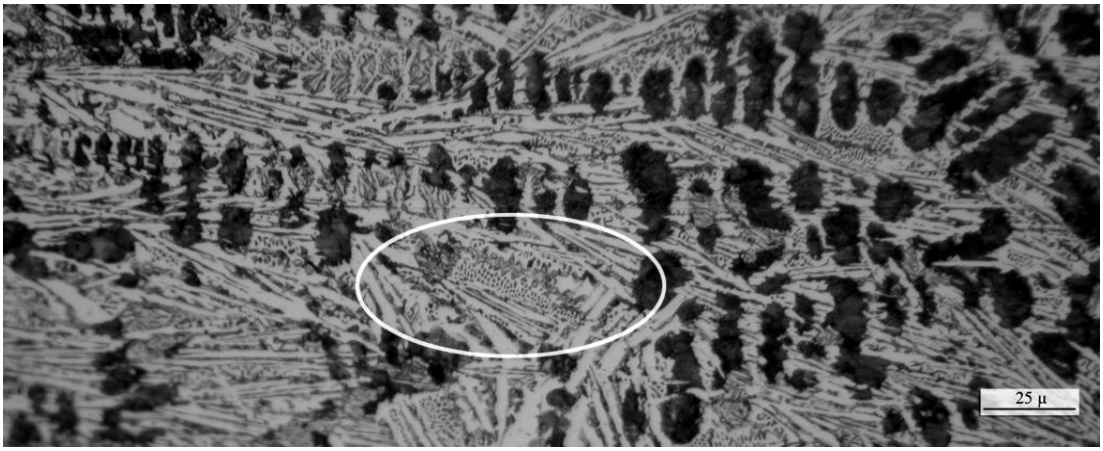

Figure 42 Ledeburitic structure among UMZ structure (as-weld). Large darker regions are martensitic dendrite arms.

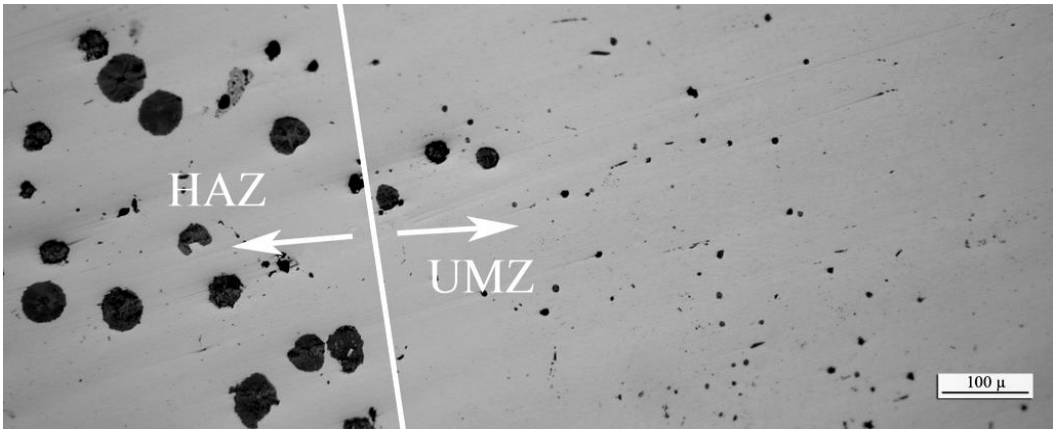

Figure 43 Graphite micro structure at UMZ (unetched). Graphite precipitation in UMZ is shown.

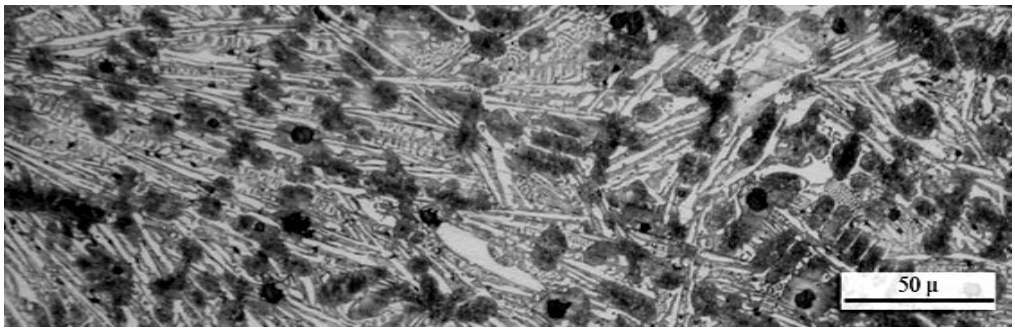

Figure 44 UMZ microstructure of the specimen PWHT at 400°C. Precipitated graphite can be seen among dendrite arms

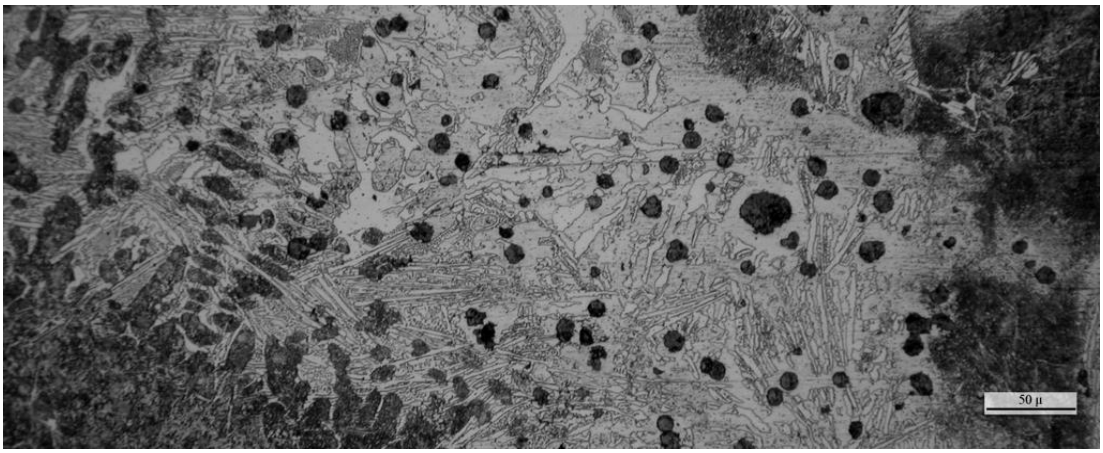

Figure 45 UMZ microstructure of specimen PWHT at 700°C. Partially decomposition of iron carbide in regions closer to PMZ can be seen.

As an overall investigation, the UMZ formed near the fusion line cannot be in any way completely eliminated by application of these heat treatments. It is possible to precipitate carbon as graphite in greater scale and formation of malleable cast iron having superior properties with respect to ledeburitic white cast iron however, this transformation requires about 30 hours or more at below eutectoid temperatures. Although cannot be eliminated, the width of UMZ can be reduced by lowering the heat input. This may be achieved by reducing the welding parameters and increasing the number of weld passes to complete the welding. By this way at single pass lower heat is introduced to the material and effect of heat can be controlled more sensitively.

5.4.2.2.2 PMZ

PMZ forms neighboring UMZ as a border to HAZ. Complete melting does not occur in this region, the temperature reaches to values between the eutectic temperature and the liquidus temperature of the cast iron. Again because of the melting and the high cooling rates, white cast iron forms. Formation of structures in this region is dominated by carbon diffusion out from the graphite.

Figure 46 can be used to characterize the PMZ of the cast piece. Partial melting temperatures in this region do not completely damage the graphite nodules. At increased temperatures, the carbon becomes capable of diffusing out from the nodules and can increase the carbon content of the neighborhood. As the carbon concentration increases, composition required for eutectic melting is reached and these regions melt. Again with the high cooling rates, the melted neighborhood transforms to white cast iron. Further away from nodules melting does not occur and these transforms to martensite constructing a martensitic hardened shell surrounding melted region. This behavior can be seen more detailed in Figure 47.

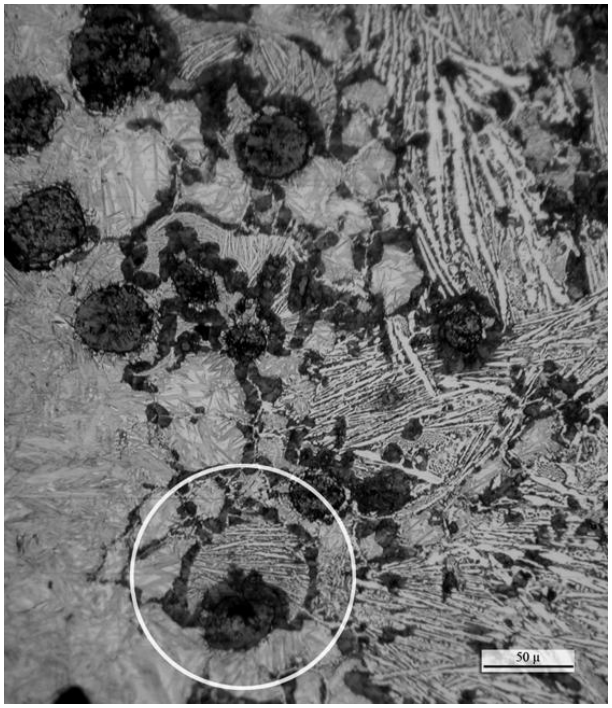

Figure 46 Microstructure of PMZ, structure near a graphite nodule is marked (magnified in Figure 47) (as-weld)

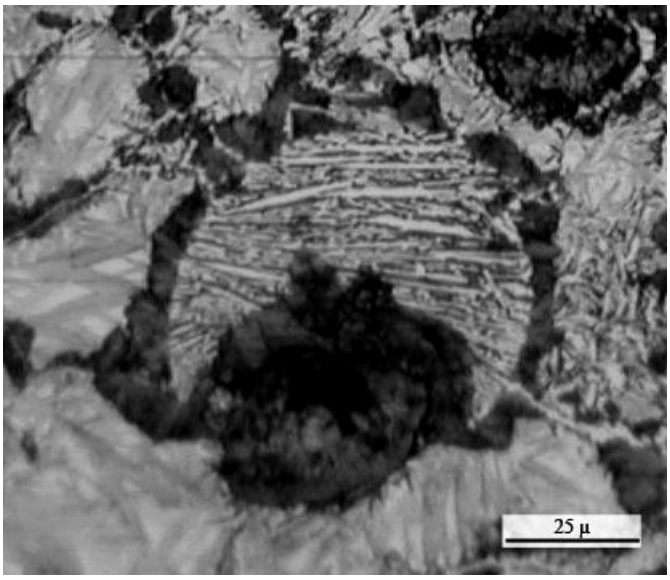

Figure 47 Detailed photograph of graphite nodule and neighborhood in PMZ (as-weld). Remelted region and martensite shell around the graphite nodule is shown.

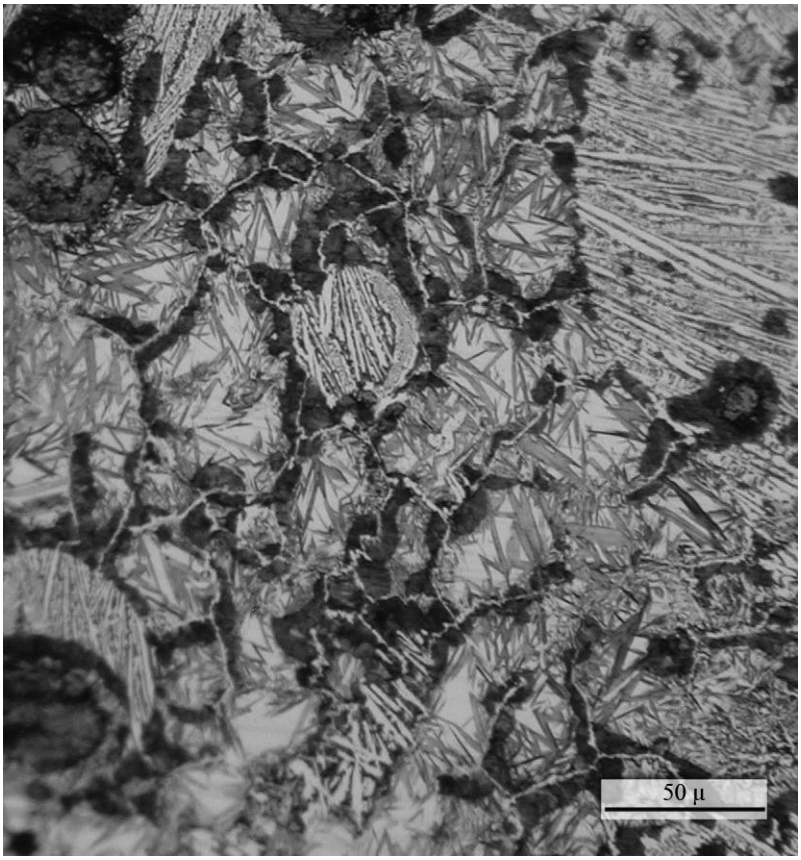

Figure 48 Microstructure of PMZ (as-weld). Ledeburitic white cast iron and acicular ferrite formation is visible in the grains

Another important characteristic of PMZ can be seen in Figure 48. In this region grains were observable. The boundaries were made up of the cementite covered by the same dark martensitic shell mentioned above. It was also seen, the matrix could be white cast iron or acicular ferrite. In the melted grains, white cast iron formation occurs, whereas without melting, the combined effect of preheating and welding acts like austempering and cause formation of acicular ferrite in this region.

Under the effect of PWHT at 400°C the PMZ to HAZ transition becomes smoother. The dark martensitic shells lost their contrast and acicular ferrite formation is no longer visible (Figure 49) due to tempering. Grains were still vaguely visible. A more detailed view (Figure 50) shows a minor bull's-eye formation. The hardened still a shell surrounding the white cast iron and ferrite around the graphite nodules can be seen.

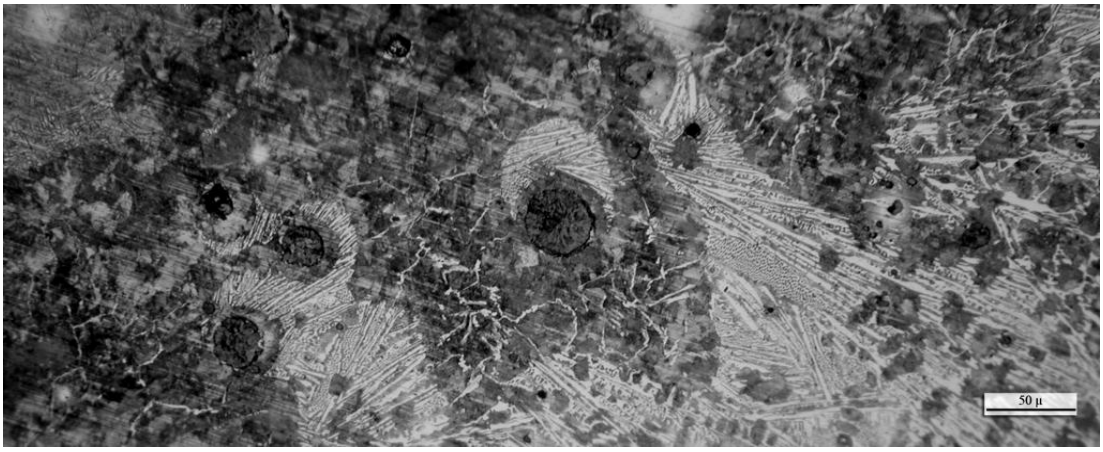

Figure 49 PMZ microstructure of the specimens PWHT at 400°C

By increasing the heat treatment temperature, martensite and hardened shells were no more visible. Same transformation as in the UMZ was seen here, high temperature tempering decomposes the pearlite and carbon present grows on the existing graphite, by this way the graphite nodules and white cast iron get surrounded by ferrite. The rest transforms into very fine pearlite (Figure 51).

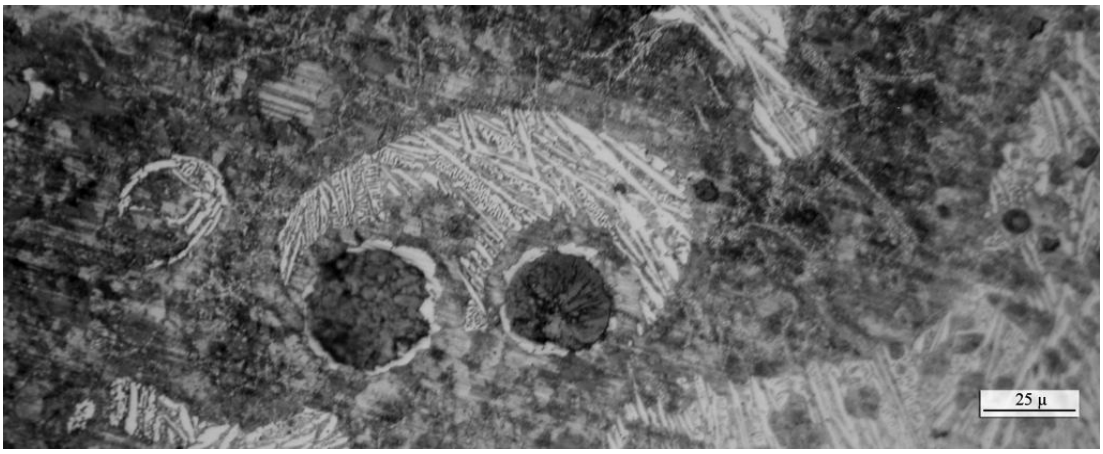

Figure 50 PMZ microstructure of the specimens PWHT at 400°C (Greater magnification)

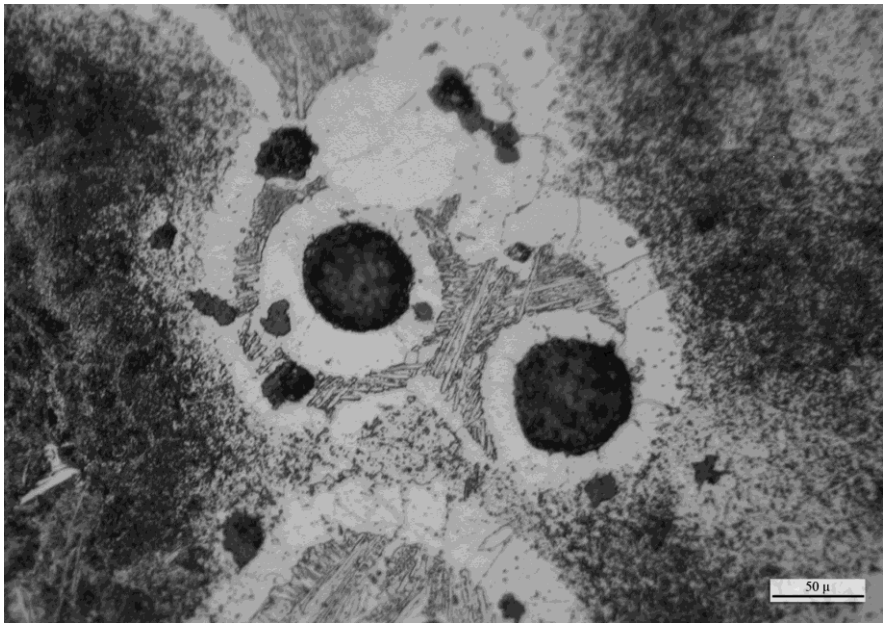

Figure 51 PMZ microstructure neighboring graphite nodules of the specimens heat treated at 700°C

5.4.2.2.3 HAZ

The HAZ reaches to temperatures between the eutectoid and eutectic upon cooling. No melting occurs. General view of HAZ in the as-weld specimen is shown in Figure 52. The regions close to the PMZ yields fully martensitic matrix with graphite nodules. As distance from the PMZ increases the cooling rate also decreases thus the

amount of martensite decreases leaving ground for pearlite and ferrite. Just outside of HAZ undisturbed bull's eye structure was examined. Additionally, as in PMZ, acicular ferrite forms at the PMZ boundary. The martensitic region just outside of PMZ can be seen in Figure 53. On this figure acicular ferrite formation can distinctly be seen at the PMZ boundary (the right edge of the figure). With the application of heat treatments same transformations took place related to constituents of UMZ and PMZ. Fully martensitic regions got tempered and by increased temperature it was possible to dissipate all the martensite in the structure (Figure 54). One additional mechanism here was formation of secondary graphite which occurs as a result of decomposition of martensite. Secondary graphite formation is clearly visible in Figure 55.

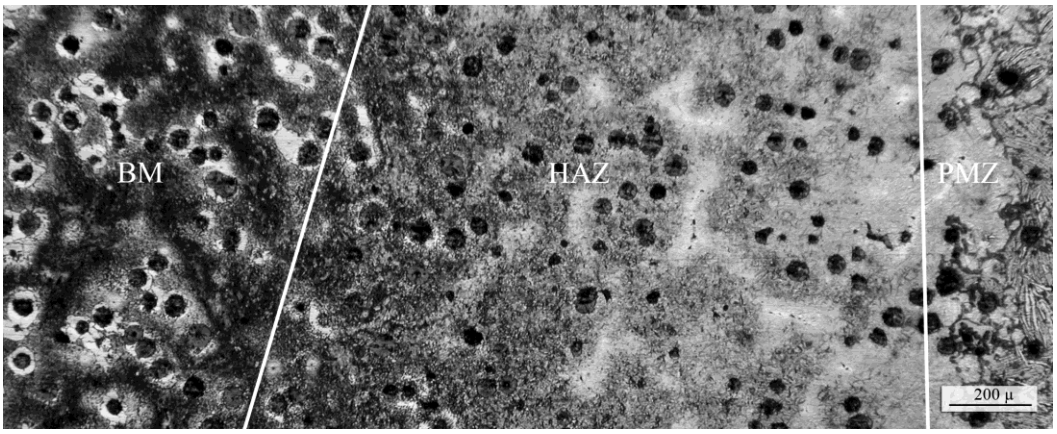

Figure 52 Microstructure variations in HAZ of an as-weld specimen

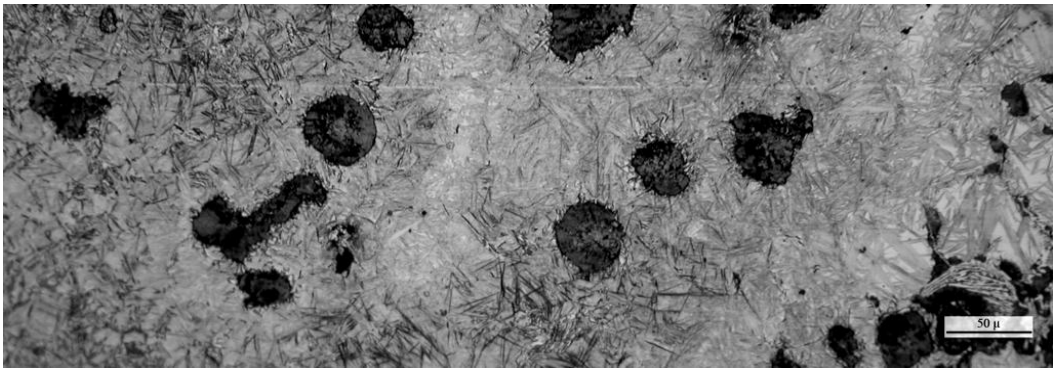

Figure 53 Martensitic HAZ microstructure near PMZ. Acicular ferrite formation is also visible at the right edge of the figure, at the PMZ boundary (as-weld)

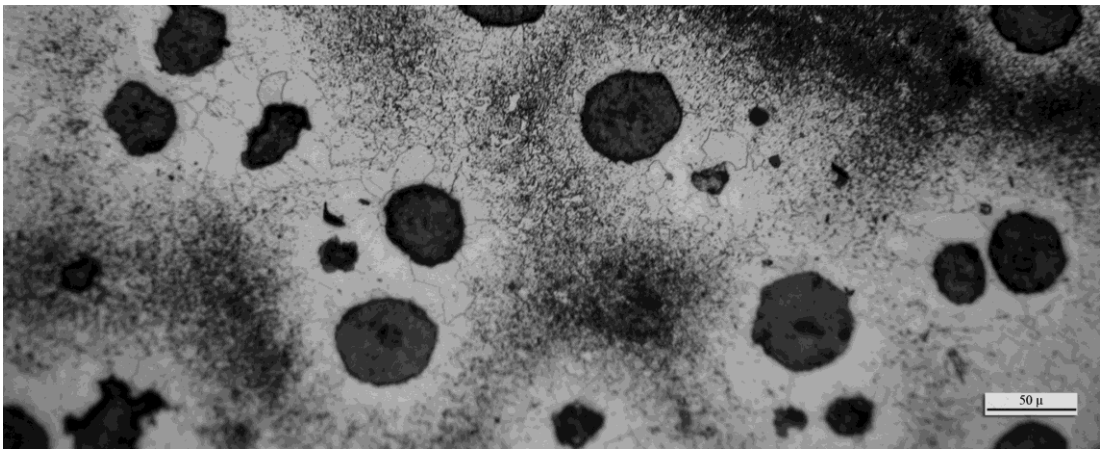

Figure 54 Ferritic-pearlitic structure. All martensite is decomposed (PWHT at 700°C)

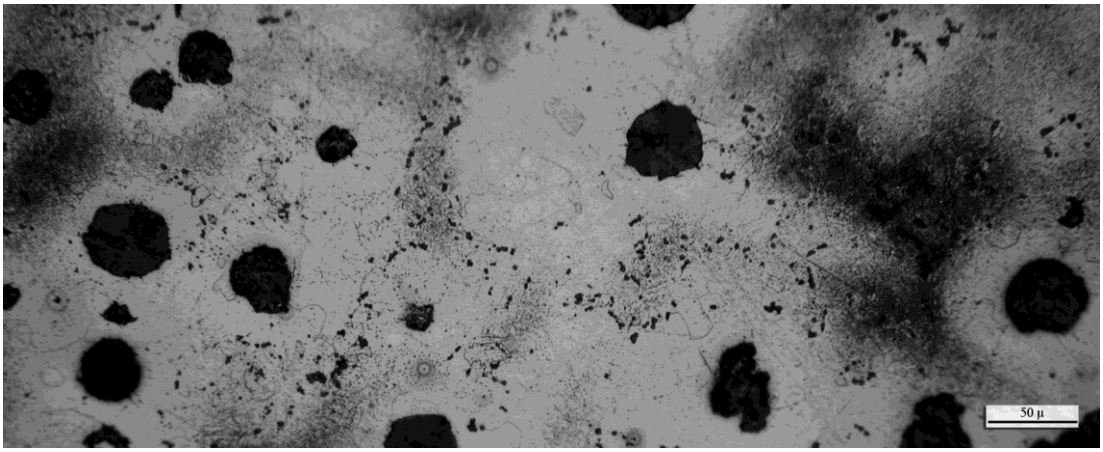

Figure 55 HAZ PWHT at 700°C. Ferritic matrix with very fine pearlite and secondary graphites are observable

5.4.2.2.4 Micro Hardness Tests

For additional characterization micro hardness tests have been carried out. The changes of hardness of dendrite arms and carbides of UMZ and remelted regions and acicular ferrite of PMZ with respect to heat treatments were determined and tabulated in Table 8.

As shown, martensite and carbides cause a great increase in hardness. Values reaching over 800 HV were determined. By the heat treatment it was possible to

lower hardness of all the regions gradually by the increase in temperature. The martensitic dendrites endure heat treatment with relatively small change. Even if all the martensite in this region gets tempered by the heat treatment, this will result formation of very fine pearlite and again hardness of this region will be very high. Hence it is not surprising to come across with small reduction of hardness in this region. No distinct reduction of hardness in interdendritic and remelted regions was seen tempering at 400°C due to the iron carbides in these regions however; by heat treatment at 700°C, hardness at these regions lowers more than 300HV. This decrease shows that partially decomposition at these regions can effectively lower the hardness. Additionally hardness values lower than 200HV in PMZ is again supportive for ferritizing in these regions.

Table 8 Hardness values of structures of UMZ and PMZ

	UMZ						PMZ					
	Dendrite arms			Interdendritic regions			Remelted regions			Acicular ferrite		
As-weld	527	558	619	642	693	777	664	551	687	612	670	683
PWHT at 400°C	557	695	642	844	757	669	584	571	476	399	551	538
PWHT at 700°C	417	382	393	298	376	326	319	301	322	135	178	177

It can be concluded that, the welding route used in this study introduces locally hardened layers with values reaching over 800HV. This hardness can be lowered to reasonable values by heat treatment at 700°C but again it is not possible to modify the hardness of these regions completely. As mentioned above complete modification of the microstructure cannot be achieved by these heat treatment methods.

5.5 Mechanical Tests

For characterization of the mechanical properties, hardness, tensile, impact and fatigue tests were applied and general mechanical behavior was determined.

5.5.1 Hardness Tests

In order to sketch out the hardness characteristics of the weld pieces, three specimens taken out from different weld plates for each heat treatment conditions and for the as-weld state and these were subjected to the hardness tests explained in experimental

procedure section. Since cast side does not construct a regular fusion line, the hardness measurements for fusion line were taken from UMZ close to PMZ. The results of the hardness tests were tabulated in Tables B1, B2 and B3 of Appendix B.

In these tables the distribution among the HAZ of two materials were given. The base materials' hardness values changes between 150-170HV, 200-250HV for E355 and GJS600-3 respectively. The general hardness distribution of the specimens in as-weld condition and heat treated conditions can be seen in Figure 56**.**

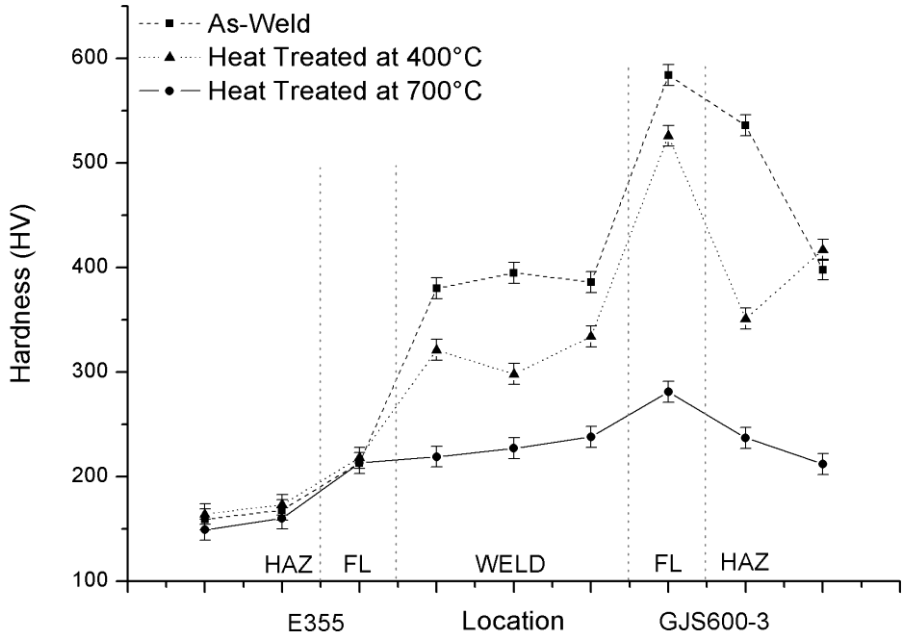

Figure 56 Hardness distribution of the joint weld in as-weld state and heat treated conditions

In the as-weld condition the hardness distribution shows a large variation at regions between two base metals. At steel side, reaching to the weld metal, hardness did not show a critical change. However; in the weld region it reaches to values over 350HV and when GJS600-3 fusion line was reached values about 575HV were observed. In HAZ hardness got values between 350 and 600HV. Specimens tempered at 400°C result lower hardness values at weld metal and fusion line with a decrease at the range of 50HV. Weld hardness decreases to values below 350HV but hardness above

500HV was witnessed at fusion line. Tempering at 700°C provides a smoother and lower hardness distribution lowering all the values below 300HV.

When a comparison with the results of the microstructural and micro hardness studies is carried out, these hardness distribution mentioned above make more sense. The hardness of weld metal and HAZ of cast iron is directly related to the martensitic structure of these regions. The decrease of hardness at these regions is due to tempering of the martensite. The high hardness of fusion line is caused by formation of white cast iron and acicular ferrite at transition region between UMZ and PMZ. Heat treatment at this region partially decomposes the iron carbide in white cast iron and dissipates the acicular ferrite formation. These two transformations in combination favor the decrease in hardness. Because 400°C is insufficient for decomposition of iron carbide, the decrease of hardness in 400°C PWHT case is relatively low.

When these findings are summarized, it may be said that as-weld specimens show a very harsh hardness variation through the cross-section. It is seen application of PWHT at 400°C provides some tempering and a parallel decrease in hardness but it is insufficient for softening the fusion line. On the other hand, application of PWHT at 700°C decreases all the hardness values under 300HV and a more homogeneous hardness distribution changing between 150-300HV can be achieved. But although in macro scale it seems hardness can be lowered below 300HV, it should be noted that as shown by micro hardness tests there are regions still having very high hardness values.

5.5.2 Impact Toughness Tests

Characterization of impact properties of the weld was done upon testing the weld metal and E355 fusion line impact properties. Pearlitic cast irons are not expected to be used under impact loads but in order to see the general impact characteristics, impact test is applied to both sides. Impact notches were introduced into the weld metal and over the fusion lines. Fusion line notches passes through weld metal and HAZ and thus represents the impact characteristics of the joint at base metal interfaces. The impact values are given in Table 9.

Table 9 Impact energies (in Joules) of weld joint with respect to the heat treatment conditions and notch locations. The data is normalized for easier comparison.

	Notch locations		
	GJS600-3 Fusion Line	**Weld**	**E355 Fusion Line**
AW 1	4.21	133	189
AW 2	5.28	43	48
PWHT400-1	4.38	56	126
PWHT400-2	3.77	89	37
PWHT700 1	7.54	21	180
PWHT700-2	3.26	73	38

The cross-sections of the specimens changes between 30-40mm^2 due to machining for specimen preparation. Since energy absorbed is directly related to the cross section, after the tests the impact toughness values are normalized as if specimens having 80mm^2 cross-section. This area is the cross-section of the most commonly used impact toughness specimen having 10x10x55mm dimensions with a 2mm of V notch introduced. According to the results, two things here should be taken into consideration; first great toughness difference between the materials and second variations at same locations of same kind of specimens.

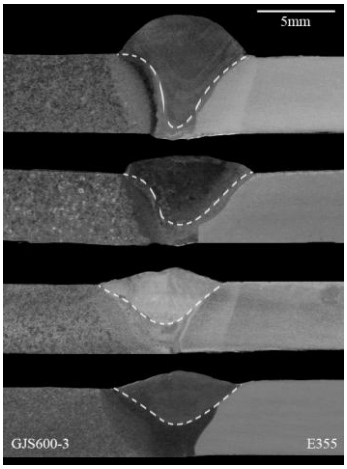

Figure 57 Macro inspection photographs of various joints in heat treated or as-weld conditions. The dashed curves on the weld metals show the boundary between first and second pass of welding.

The toughness difference between two metals is expected due to the low toughness characteristics of the pearlitic cast irons and additionally, the hard and brittle zones in neighborhood of fusion line expand this gap. The variations in same locations can be explained with the help of Figure 57. Main points to be emphasized in this figure are the cross-sectional views of fusion lines and weld beads. When fusion lines are considered it can clearly be seen in macro scale that no regular fusion geometry is obtained. Hence it is a great possibility that when the notch is introduced, the cross-section at notch location is not shared equally by weld metal and HAZ which are expected to have different toughness values. Same kind of behavior is also active in weld metal. As seen from the figures the ratio of the height of the two weld beads changes from specimen to specimen. So when a notch is introduced here, again the cross-section is divided between these two passes with different properties. This difference is born because the tempering effect of the second pass and dilution ratios according to the volumes of the passes.

The above mentioned geometrical properties are variable from location to location and expected to cause variations of data. Additionally any milimetric error on the notch location will also change the test results. Hence when designing any construction related to toughness, these points should be considered and it should be noted that the toughness values of the joint may be between 5 to 200 joules.

5.5.3 Tensile Tests

Tensile tests were applied to the base materials and to the joint pieces in order to compare the materials' mechanical behaviors before and after the welding. Additionally tensile properties of the base materials were used to specify the tensile characteristics of joint pieces.

5.5.3.1 Base Metal Tests

Base metal specimens were again tested in 3 sets. First set was tested without any processes, the second and third sets were applied the same heat treatment conditions as the tempering processes that was held at 400 and 700°C for 1 hour before testing. Stress-strain diagrams for the base metals are shown in Figure 58. Only diagrams of non-treated specimens are given here because of the similar characteristics of heat

treated ones. Mechanical data gathered from the tests were tabulated in Table 10 and Table 11. Yield and tensile stress values are graphically shown in Figure 59 both materials.

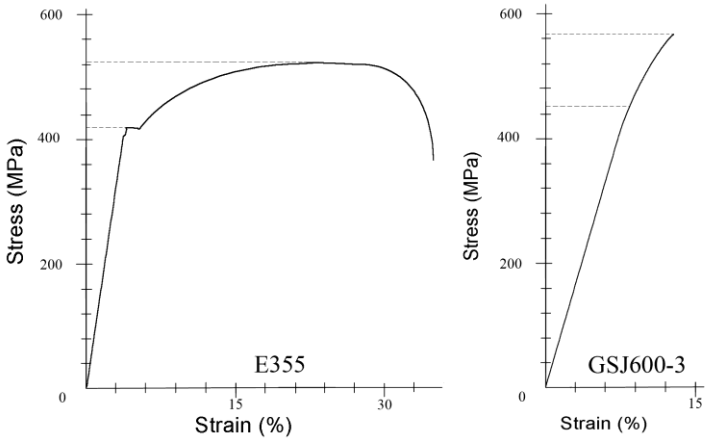

Figure 58 Stress-strain curves of E355 (left) and GJS600-3 (right) at non-treated conditions

Table 10 Tensile properties of GJS600-3 in non-treated, heat treated at 400°C and 700°C conditions. Yields are determined by 0.2 offset method.

	$R_{p0.2}$ (MPa)	R_m (MPa)	% Elongation
Non-treated-1	475	652	5
Non-treated-2	451	559	3
400°C-1	424	492	3
400°C-2	430	525	3
700°C-1	455	600	6
700°C-2	360	371	1

In both materials the tensile stresses tends to decrease with the increase in the heat treatment temperature. When yield stresses are compared, E355 shows a regular increasing behavior however; yield stress values for GJS600-3 tends to decrease by the increase of treatment temperature. The tensile and yield stress values of E355 changes in the range of 50MPa whereas for GJS600-3, especially for tensile values

the change occurs in a 100MPa range. Table 10 clearly shows this greater variation of values of GJS600-3. These fluctuations are thought to be a result of the non-homogeneous nature of the cast piece. Some casting voids are detected in the cast metals which will be mentioned in fractography section for fatigue tests.

Table 11 Tensile properties of E355 in non-treated, heat treated at 400°C and 700°C conditions. Higher yield points are tabulated.

	R_{eH} (MPa)	R_m (MPa)	% Elongation
Non-treated-1	413	515	31
Non-treated-2	418	514	25
400°C-1	448	523	24
400°C-2	438	499	25
700°C-1	477	477	28
700°C-2	434	484	25

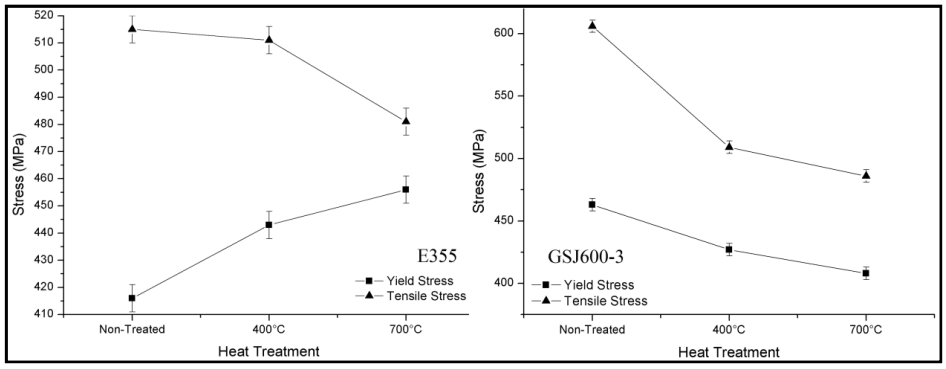

Figure 59 Tensile and yield stress variations with respect to heat treatment for GJS600-3

5.5.3.2 Weld Joints

Total number of six specimens, two for each PWHT states and two for as-weld state were tested. The diagrams can be seen in Figure 60, Figure 61 and Figure 62. It was expected to get a linear elastic behavior however, as seen from these figures; linearity in elastic region was not preserved. This curved behavior was suspected to be introduced due to measurement error. Since stroke controlled strain measurement was done, a slide of the specimens between the jaws in micron order would cause

noticeable changes in the strain behavior on the diagrams. Hence the deviation from the linearity was related to this factor.

Some irregularities were detected on the diagrams and these are marked with arrows and stress values are listed in Table 12. These irregularities are judged to be the yield stresses of different constituents and tried to be classified with the help of Table 10, Table 11, Table 12 and stress strain diagrams.

Some estimations can be done for characterization of the curve. Due to smooth elastic to plastic transition of the cast piece, it was expected to come across a change of slope of the curve rather than a distinct irregularity at the yield point. Additionally if cast piece yields after E555 or they yield simultaneously, the change due to cast piece could be undeterminable. If hardness values are correlated to yield points, yields of E355 base metal and E355 HAZ can assumed to be same. Regions with higher hardness were not expected to cause yield before the fracture due to same correlation. Weld metal of the specimens heat treated at 700°C can also create a yield point on the diagram due to lowered hardness. Also no yield was expected below 350MPa according to the cyclic stress-strain behavior of the material which will be mentioned in fatigue test section. It is not possible to name every irregularity on the diagrams certainly but with the estimations mentioned above and the values given in above tables the possibilities were specified. These possibilities are shown on Table 13. At the first irregularities of AW2 and PWHT400-2 simultaneous yielding of the materials is possible. It is highly probable for GJS600-3 yields unnoticeably on the diagrams where GJS600-3 is not listed.

In an industrial point of view, when welded joints are tested according to EN 895 standard, the only criterion deciding the success of joint for tension tests is satisfaction of the tensile stress of the weaker base metal or design criteria of the construction. According to the results of the non-treated base metals (Table 11), the weld joint average tensile stress should exceed 515MPa. This necessity is only satisfied by the as-weld specimens. With the application of heat treatments tensile stress lowers to 475MPa range. So it can be judged that this joint type for these two materials can be acceptable in as weld conditions according to base metal criteria however, if construction design allows 475MPa of tension stress, the heat treated specimens also become usable.

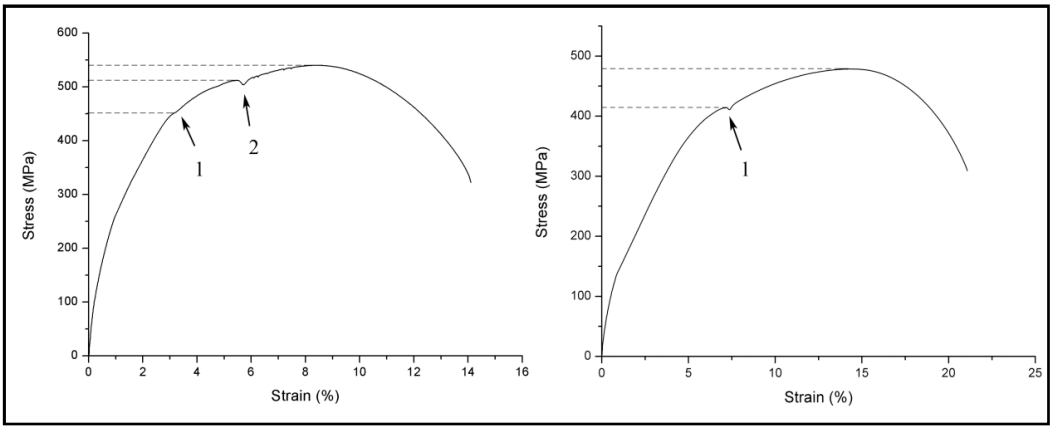

Figure 60 Stress-Strain diagrams of welded specimens in as-weld condition (AW1 at left and AW2 at right)

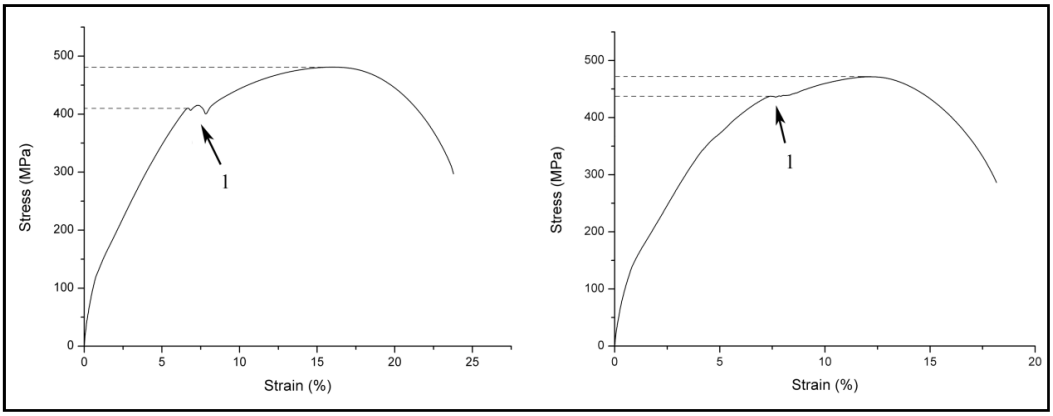

Figure 61 Stress-Strain diagrams of welded specimens tempered at 400°C (PWHT400-1 at left, PWHT400-2 at right)

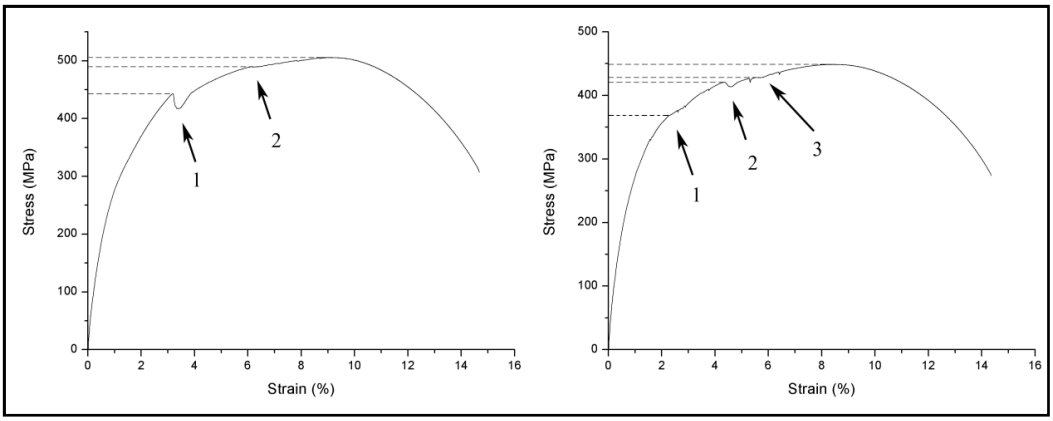

Figure 62 Stress-Strain diagrams of welded specimens tempered at 700°C (PWHT700-1 at left, PWHT700-2 at right)

Table 12 Tensile properties of welded joints in as-weld and tempered states. Stresses of irregularities (Irr.), R_m, elongation at failure and failure locations are listed

	Irr. 1	Irr. 2	Irr. 3	R_m	Elongation	Fracture Location
	(MPa)				%	
AW1	451	512	N/A	540	13.5	E355 (Base Metal)
AW2	415	N/A	N/A	480	11.7	E355 (Base Metal)
PWHT400-1	410	416	N/A	480	11.6	E355 (Base Metal)
PWHT400-2	370	437	N/A	471	11.1	E355 (Base Metal)
PWHT700-1	443	490	N/A	506	14.7	E355 (Base Metal)
PWHT700-2	370	420	429	450	12.9	E355 (Base Metal)

Table 13 Yield point estimations for the stress strain diagrams for all three states

	1st Irregularity	2nd Irregularity	3rd Irregularity
AW1	GJS600-3	E355	N/A
AW2	Can be both	N/A	N/A
PWHT400-1	E355	N/A	N/A
PWHT400-2	Can be both	N/A	N/A
PWHT700-1	E355	GJS600-3	N/A
PWHT700-2	GJS600-3	E355	Weld Metal

5.5.4 Fatigue Tests

The fatigue life of the welded joints is strongly determined by the notch effect of the weld joint and as mentioned in Chapter 2. In any ordinary welding operation the flank angle, thus the effect of geometry, changes throughout the weld length and introduces variations to fatigue service life of the elements. In order to dissipate such additional factor, the weld tips and roots were machined and a regular rectangular cross section is attained over the joint.

5.5.4.1 Fatigue Life and Failure Locations

The loads applied for the tests were selected in light of the results of tension tests. In order to see the general behavior firstly the specimens are loaded between σ_{min}= 0MPa and σ_{max}= 350MPa which is about 85% of the lowest yield stress determined on the stress strain diagrams. Numbers of cycles at failures and fracture locations are tabulated in Table 14.

Table 14 Fatigue test results

Specimen	Cycles to failure	Failure location
AW-1	102975	Base Metal (GJS600-3)
AW-2	43053	Base Metal (GJS600-3)
AW-3	116985	Base Metal (GJS600-3)
400-1	29545	Base Metal (GJS600-3)
400-2	35291	Base Metal (GJS600-3)
400-3	36475	Base Metal (GJS600-3)
700-1	96259	Base Metal (GJS600-3)
700-2	101212	Base Metal (GJS600-3)
700-3	38546	Base Metal (GJS600-3)

At this stage a characterization about the fatigue lives of the specimens cannot be done. When Table 14 is examined it may be said that in average, fatigue life decreases in 700°C tempered - as weld - 400°C tempered order but it is always expected to come across with serious scatter of the fatigue life data of any material. In order to make a consistent characterization, statistical analysis over a large group of specimens having identical properties should be carried out. However; it is nearly impossible to achieve such a specimen group in this case. The weld joint consists of three components all having their own fatigue characteristics. In addition to the base and filler materials, the phases created during welding (HAZ, UMZ, PMZ) and fusion lines behave like additional components with additional features. The overall fatigue properties of all these components vary from location to location on a welded plate because of the nature of welding. Additionally, all properties of the mentioned components change with respect to the applied heat treatments. All these things mentioned create an ocean of possibilities for increasing of data scatter. Because of these reasons, a judgment related to the fatigue lives of the joints cannot be done with this limited number of specimens.

However, the main point here to attract attention is the failure locations of the specimens. As shown in Table 14 all fatigue test specimens have failed from the GSJ600-3 base metal independent of the cycle count. That is, in tensile fatigue test cast piece becomes the weakest link and determines the joint behavior under cyclic loads.

5.5.4.2 Cyclic Stress Strain Behavior

Although a load lower than the yield points of the materials was selected for fatigue tests, possibility of plastic deformation was suspected due to the very short service lives under cyclic loads. For this reason cyclic stress strain behavior of an as-weld (AW-3) specimen was sketched by using data points following 20000^{th}, 60000^{th} and 100000^{th} cycles. These data points are shown in Figure 63.

The distribution of the data shows elliptic stress-strain behavior as seen on stress strain diagrams of the specimens. At first look all the curves seem identical to each other. To define possible misfits, mean lines of the ellipses were drawn and the slopes were calculated. As seen in Table 15, the diagrams have come off with very similar slopes which can assumed to be identical. This behavior shows that the materials follow the same path till the failure that no plastic deformation occurs. This also confirms that no regions yield under 350MPa.

Table 15 Slopes of the mean lines of cyclic stress-strain diagrams of Figure 63

Cycles	20000	60000	100000
Slopes (GPa)	61.413	59.333	61.000

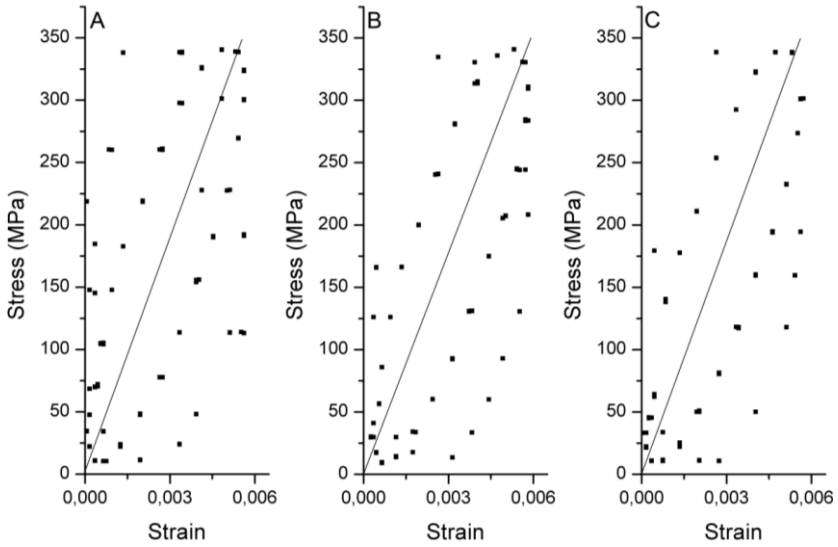

Figure 63 Stress-strain behaviors during fatigue test. (A. 20000 cycles, B. 60000 cycles and C 100000 cycles)

5.5.4.3 Fractography

A characterization of fracture behavior was done. It was seen that all specimens have failed from GJS600-3 side, from base metal well away from effects of the weld. To see the details of the general fracture behavior of the material, fractography studies were carried out under scanning electron microscopy. In all materials for all conditions same characteristics were determined. It was observed that the cracks start to form from corner of the cast piece. Complete failure occurs by fatigue fracture followed by fast fracture mechanism. The starting location and transition to fast fracture is shown on Figure 64.

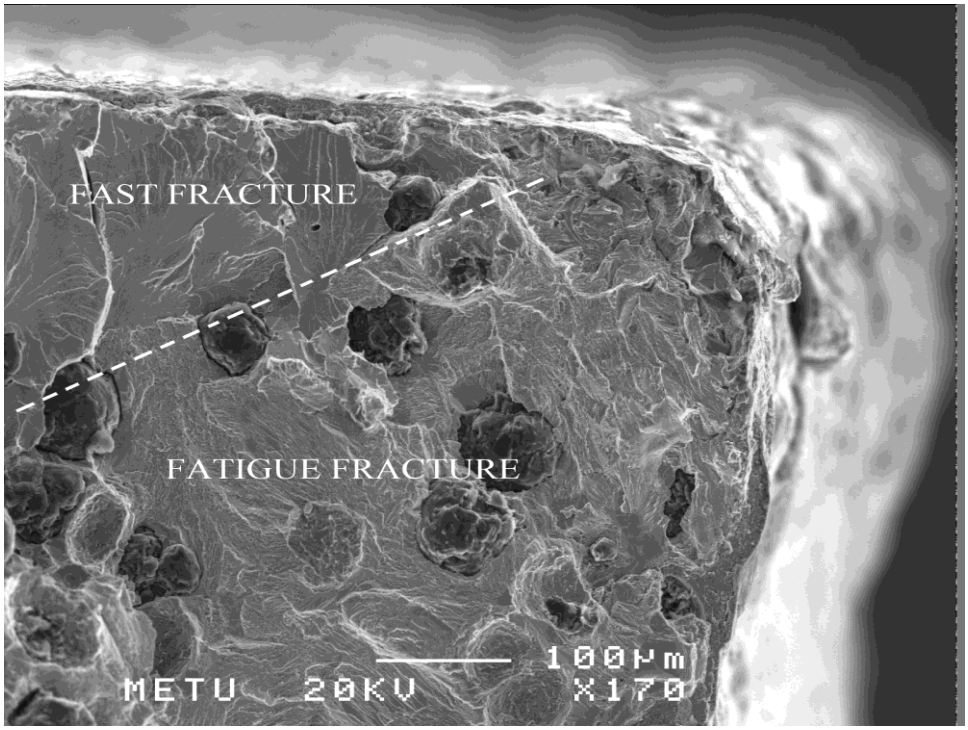

Figure 64 Crack starting location of cast piece. Fatigue and fast fracture regions of specimen AW1 are shown

In fatigue fracture region, crack propagation is controlled by the pearlitic structure of the cast piece. This behavior can be seen in more detail in Figure 65. When the crack grows the load bearing cross section gets smaller and smaller and after a critical point fast fracture occurs. This transition point between the fatigue fracture and fast

fracture can be witnessed in Figure 66. Here the crack penetrates into the neighboring grain and the penetrated grains fail to bear the loads and gives way in a brittle manner. A completely fast fractured surface that occurs beyond this point can be examined in Figure 67. In both fracture types the failure occurs in a brittle manner, nearly no deformation can be witnessed.

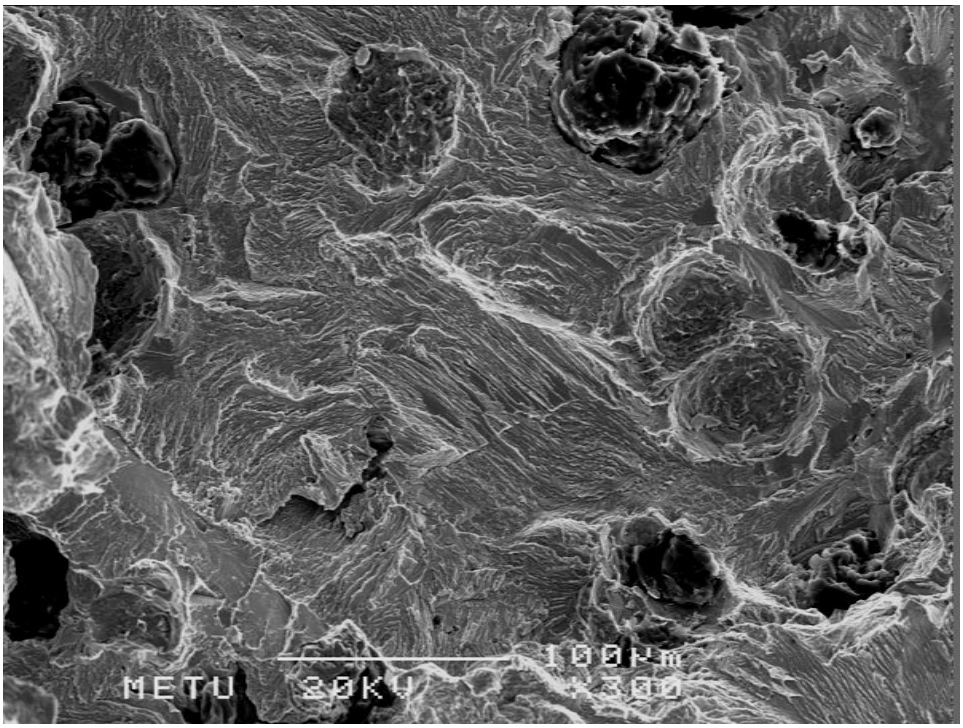

Figure 65 Pearlitic structure on the fracture surface of specimen PWHT700-3

In some regions casting voids were determined. These voids could be located in the bulk or near the surface and identified as crack start points. Figure 68 shows one of these voids at the corner very close to the surface. Dendritic cast structure can be determined here. Around the void same crack characteristics mentioned above were detected. These voids act as stress concentrators and determine starting location of cracks and also lower the fatigue life. In two of the specimens heat treated at 400°C such voids were determined. Respectively lower service life of this set is related to existence of voids.

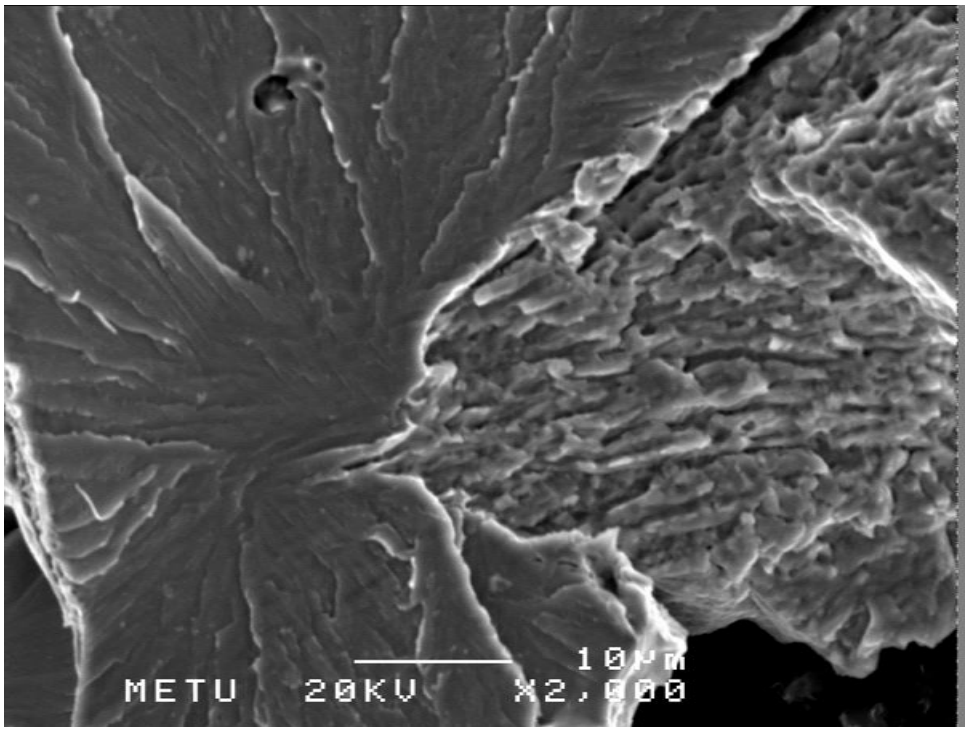

Figure 66 Fatigue fracture (right) penetrates into neighboring grain (left) on specimen PWHT700-3

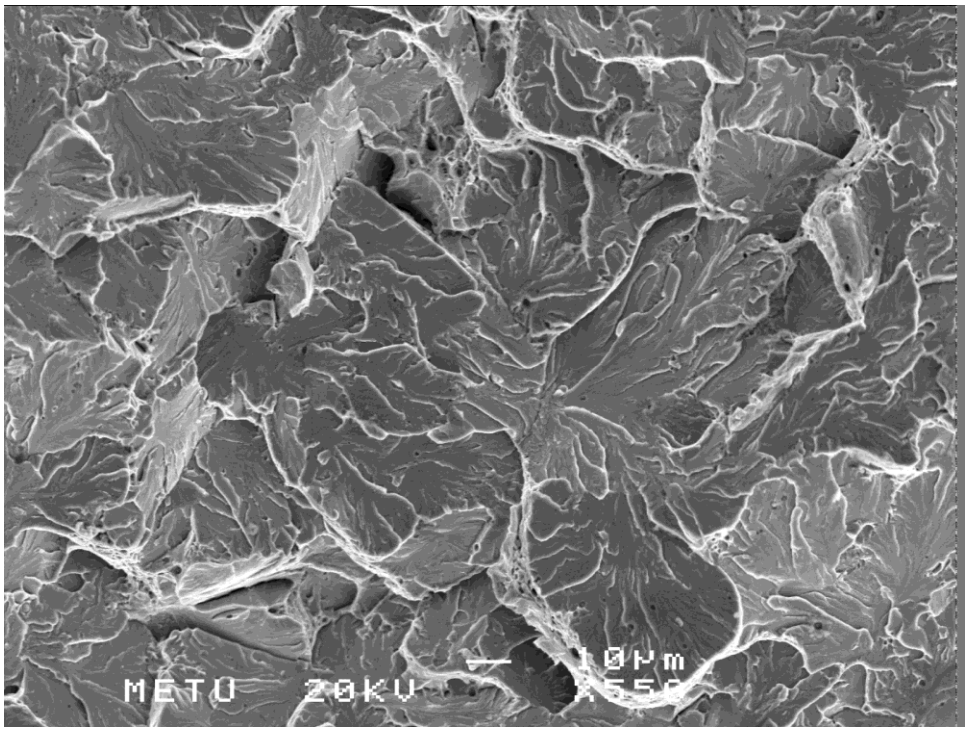

Figure 67 Fast fracture region on specimen AW-2

In overall, GJS600-3 becomes the determining factor for fatigue behavior under the cyclic load conditions indicated above. The joint fails at regions away from the effect of welds. The welding joint and steel piece becomes superior to the cast piece in all conditions. It was also seen, fatigue behavior was independent of the heat treatment conditions. Additionally, existence of casting voids in the cast structure can be capable of dominating the overall fatigue properties and hence certain classification regarding the fatigue life cannot be done.

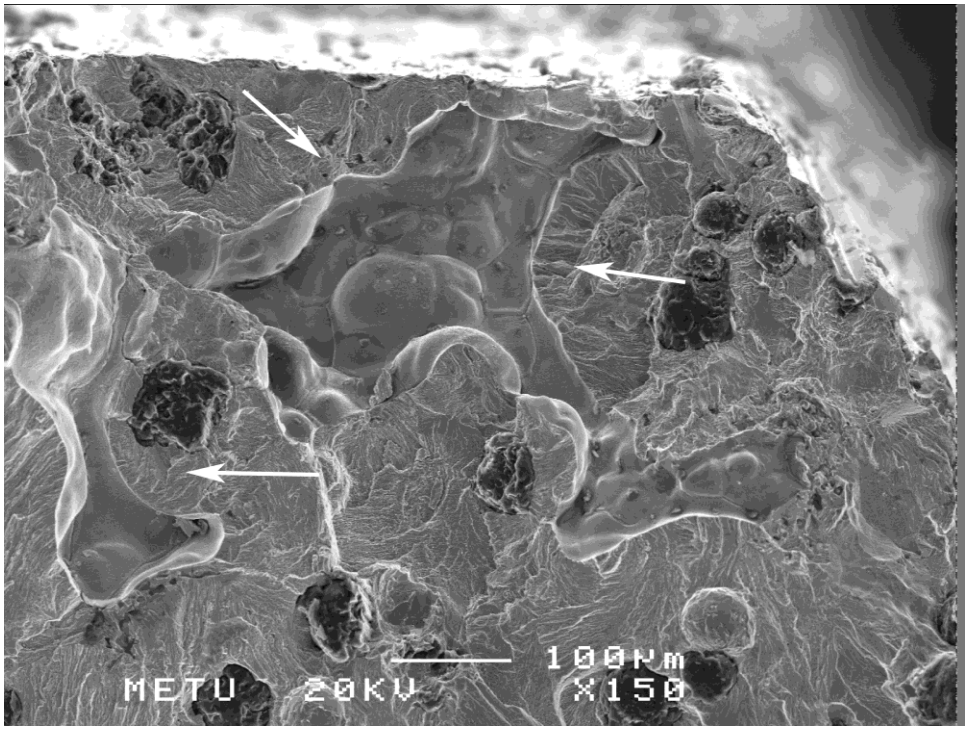

Figure 68 Casting void near surface, marked by arrows (Specimen PWHT400-2)

5.6 Future Works

Up to this point general discussion about the weld joint between GJS600-3 nodular cast iron and E355 low carbon steel is discussed. General characterization of the microstructures was determined and mechanical behaviors were identified. To improve the study further certain steps may be taken.

First thing to take into consideration is sustaining preheating temperature after welding to provide sufficient time for diffusion of carbon atoms which will prevent

formation of martensite in HAZ and PMZ and also decrease the amount of white cast iron formation. By this step the hardness gradients would be lowered and post weld heat treatments might be unnecessary.

As often used in welding of cast irons, Ni based filler materials can be used. By addition of Ni into structures formation of iron carbide can be prevented up to a degree and by relatively soft nature of nickel, the tolerance for cooling cracks can be increased. This may even lift the necessity of preheating. Despite these advantageous properties, nickel based fillers constitute weaker joints and thicker welds may be required for same design criteria and probability of formation of weld defects would be increased. Additionally Ni based fillers cost higher with respect to the commonly used steel fillers.

Another thing to take into consideration may be modification of the microstructure of the cast piece. By ferritizing annealing, the pearlitic microstructure may be changed to ferrite. By this process cast piece having higher elongation capabilities can be produced and also some toughness increase can be achieved. This would narrow the gap between steel and cast pieces in mechanical perspectives. But elongation and tension properties should be taken into consideration. Ferritic nodular cast irons generally show elongation about 10-15% which will be about half of the steel piece. If by ferritizing, tension strength of the cast piece also gets lower than the steel, that may result an amount of elongation loss at fracture. Additionally by ferritizing, the fatigue fracture behavior would be modified in a more favorable direction. A ductile fracture mechanism could be introduced and service life may be increased.

Examination of fatigue behavior might also be detailed. Application of different stress ratios and changing frequency of the tests would change the general characteristics. Additionally application of these tests in tension compression manner would also show effect of compressive forces on fatigue life of the specimens. In this method hardness gradients may play important roles determining the service life.

Other methods or steps can also be applied to expand the mechanical property characterization perspective but these mentioned methods are the basic ones that may be applied in this testing route.

CHAPTER 6

CONCLUSIONS

Following conclusions can be drawn from the results of the study:

1. Nodular cast iron and low carbon steel can successfully be fusion welded using low carbon steel filler electrode but to prevent cooling cracks, suitable preheating should be applied.

2. Post weld heat treatment was successful for lowering the hardness distribution and controlling the microstructure. Post weld heat treatment on the other hand, did have no effect on the fracture location and behavior.

3. Weld metal and HAZ act superior to base metals under tension and fatigue tests. That is, fractures occur at base metals away from the effects of the weld.

4. Tensile test of the welded specimens causes failure at steel side with considerable elongation whereas fatigue test results brittle fracture of cast iron side.

REFERENCES

1. Messler R. W., Joining of Materials and Structures: From Pragmatic Process to Enabling Technology, 2004, Butterworth-Heinemann
2. Cary H. B. and Helzer S., Modern Welding Technology, 2004, Prentice Hall
3. Blondeau R., Metallurgy and Mechanics of Welding: Processes and Industrial Applications, 2008, Wiley-ISTE
4. ASM Metals Handbook. Properties and Selection: Irons, Steels and High Performance Alloys. Vol. 1. 2005: ASM International
5. Martin J. W., Materials for Engineering, 2006, Maney Publishing
6. ASM Metals Handbook. Metallography and Microstructures. Vol. 9. 1985: ASM International
7. Callister W. D., Materials Science and Engineering: An Introduction, 1994, John Wiley & Sons Inc.
8. ASM Metals Handbook. Welding, Brazing and Soldering. Vol. 6. 1993: ASM International
9. AWS Welding Handbook. Welding Processes. Vol 2. 1991, American Welding Society
10. Galvery W. L. and Marlow F. B., Welding Essentials, 2007, Industrial Press Inc.
11. Kou S., Welding Metallurgy, 2003, John Wiley & Sons Inc.
12. ANSI/AWS D11.2-89, Guide for Welding Iron Castings, 1989, American Welding Society

13. Messler R. W., Principles of Welding: Processes, Physics, Chemistry, and Metallurgy, 1999, Wiley-VCH

14. Lassen T. and Recho N., Fatigue Life Analysis of Welded Structures, 2006, Wiley-ISTE

15. Pascual M., et al., Analysis of the weldability of ductile iron. Materials Letters, 2008. 62: p. 1359-1362.

16. El-Banna E. M., Effect of preheat on welding of ductile cast iron. Materials Letters, 1999. 41: p. 20-26

17. El-Banna E. M., et al., Study of restoration by welding of pearlitic ductile cast iron. Materials Letters, 2000. 42: p. 311-320

18. Pouranvari M., On the weldability of grey cast iron using nickel based filler metal. Materials and Design, 2010. 31: p. 3253-3258

19. Voigt R. C., et al., A study of heat-affected zone structures in ductile cast iron. Welding Journal, 1983 March: p. 82-88

20. Hatate M., et al., Bonding characteristics of spheroidal graphite cast iron and mild steel using electron beam welding process. Vacuum, 2004. 73: p. 667-671

21. Sanghoon K., et al., Cracking behavior in a dissimilar weld between high silicon nodular cast iron and ferritic stainless steel. Metals and Materials International, 2010. 16: p. 483-488

22. Grum J., Sturm, Comparison of measured and calculated thickness of martensite and ledeburite shells around graphite nodules in the hardened layer of nodular iron after laser surface remelting. Applied Surface Science, 2002. 187: p. 116-123

23. Benyounis K. Y., et al., Surface melting of nodular cast iron by Nd-YAG laser and TIG. Journal of Materials Processing Technology, 2005. 170: p. 127-132

24. Xue H.Q., Damage mechanism of a nodular cast iron under very high cycle fatigue regime. Journal of Materials Processing Technology, 2008. 202: p 216-223

25. Cavallini M., Fatigue crack propagation damaging micromechanisms in ductile cast irons. Engineering Fracture Mechanics, 2008. 75: p. 694-704

26. EN 1563, Founding – Spheroidal graphite cast irons, 1997, European Committee for Standardization

27. EN 10297-1, Seamless circular steel tubes for mechanical and general engineering purposes – Technical delivery conditions – Part 1: Non-alloy and alloy steel tubes, 2003, European Committee for Standardization

28. ISO 14341, Welding consumables - Wire electrodes and weld deposits for gas shielded metal arc welding of non alloy and fine grain steels, 2010, International Organization for Standardization

29. Askaynak, on-line, http://www.askaynak.com.tr, 2003, last visited on 19/08/2009

30. EN 1043-1, Destructive tests on welds in metallic materials – Hardness testing – Part 1: Hardness test on arc welded joints, 1995, European Committee for Standardization

31. EN 895, Destructive tests on welds in metallic materials – Transverse tensile test, 2009, European Committee for Standardization

32. EN 875, Destructive tests on welds in metallic materials - Impact tests - Test specimen location, notch orientation and examination, 1995, European Committee for Standardization

33. ASTM E 112, Standard test methods for determining average grain size, 1996, ASTM International

APPENDIX A

GRAIN SIZE MEASUREMENT RESULTS

Results of the grain size measurements are given in Tables A1 to A3.

Table A1 Base metal grain size measurement data for as-weld state.

		Line length (μ)	Intercept Count	Avg. Int. Length (μ)
Image 1 (100x)	l_x	601	121	4.89
	l_y	672	118	5.61
	l_z	899	103	8.61
Image 2 (100x)	l_x	610	90	6.68
	l_y	663	87	7.51
	l_z	652	93	6.92
Image 3 (200x)	l_x	302	75	4.03
	l_y	377	82	4.60
	l_z	399	78	5.12
Image 4 (200x)	l_x	315	92	3.43
	l_y	346	82	4.23
	l_z	393	70	5.62

Table A2 Base metal grain size measurement data for 400°C tempered state

		Line length (μ)	Intercept Count	Avg. Int. Length (μ)
Image 1 (100x)	l_x	703	145	4.87
	l_y	775	103	7.53
	l_z	656	129	5.08
Image 2 (100x)	l_x	636	114	5.77
	l_y	778	88	8.84
	l_z	863	137	6.24
Image 3 (200x)	l_x	325	75	4.34
	l_y	460	98	4.71
	l_z	426	102	4.17
Image 4 (200x)	l_x	347	82	4.23
	l_y	427	86	4.97
	l_z	395	73	5.41

Table A3 Base metal grain size measurement data for 700°C tempered state

		Line length (μ)	Intercept Count	Avg. Int. Length (μ)
Image 1 (100x)	l_x	638	118	5.39
	l_y	823	101	8.16
	l_z	841	109	7.72
Image 2 (100x)	l_x	679	123	5.53
	l_y	806	98	8.15
	l_z	781	126	6.20
Image 3 (200x)	l_x	352	78	4.52
	l_y	440	71	6.21
	l_z	387	74	5.24
Image 4 (200x)	l_x	344	76	4.53
	l_y	429	71	6.05
	l_z	420	83	5.07

APPENDIX B

HARDNESS MEASUREMENT RESULTS

The hardness measurement results of the Vickers Hardness Tests are given in Tables B1 to B3.

Table B1 Hardness measurements of as-weld specimens. All values are HV.

E355						GJS600-3		
HAZ		FL		WELD		FL	HAZ	
		194				716		
157	169	238	353	370	322	813	493	313
		238				713		
		185				513		
157	165	213	354	350	384	511	633	536
		178				553		
		217				481		
162	170	204	435	466	451	478	535	346
		253				486		

Table B2 Hardness measurements of specimens heat treated at 400°C. All values are HV.

E355						GJS600-3		
HAZ		FL		WELD		FL	HAZ	
		181				500		
163	182	233	380	376	385	618	312	410
		256				657		
		204				375		
158	162	195	239	248	270	462	364	435
		222				546		
		278				473		
169	174	205	345	382	346	575	377	407
		185				534		

Table B3 Hardness measurements of specimens heat treated at 700°C. All values are HV.

E355						GJS600-3		
HAZ		FL		WELD		FL	HAZ	
		198				294		
156	160	213	224	233	236	272	197	211
		261				252		
		173				235		
130	146	185	189	209	255	356	322	199
		176				273		
		256				314		
160	175	217	243	238	223	276	192	226
		236				262		